Roles of the Lenses

Gun Lens

Helps form probe

Condenser Lens

Mainly controls:
Spot Size
hence total beam current

Objective Lens

Mainly control probe focus

Diffraction/Intermediate Lens

Controls Mode

Projector Lens

Magnification

Most TEM/STEM have 7-8 Lenses

2 Condensers
1 Objective
1-2 Intermediate
2 Projectors

Most instruments have only Electromagnetic Round Lenses

Note the locations of the various Apertures.

Optimum aperture sizes are needed for various imaging functions.

Transmission Electron Microscopy

Conventional Imaging

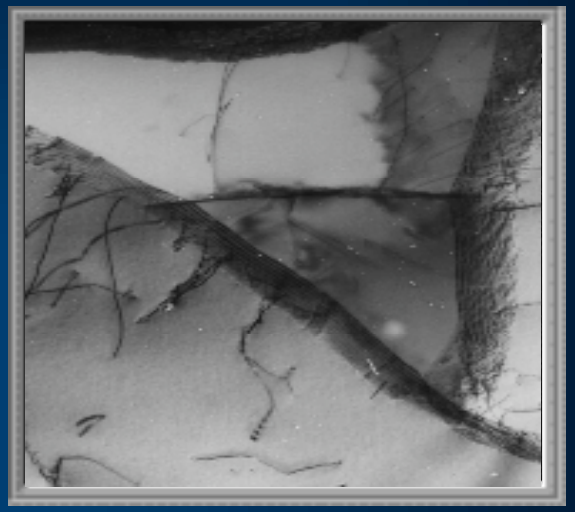

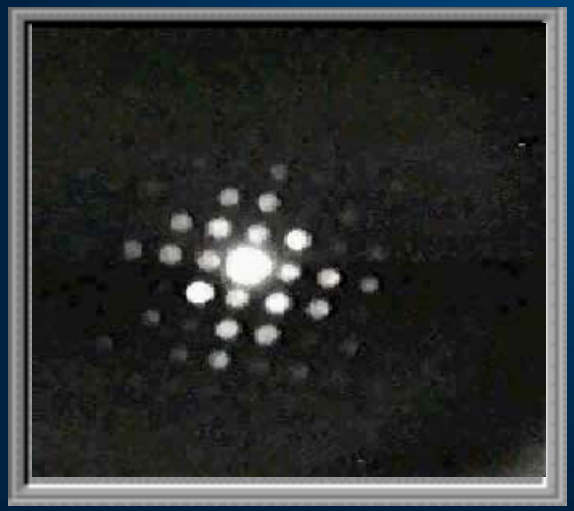

High Resolution Imaging

Diffraction

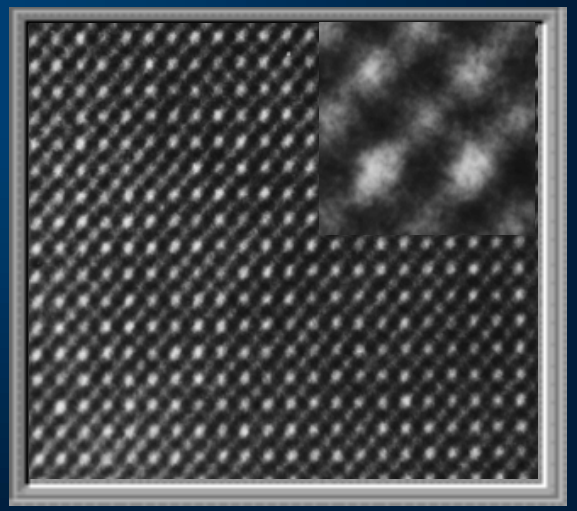

Electron Diffraction

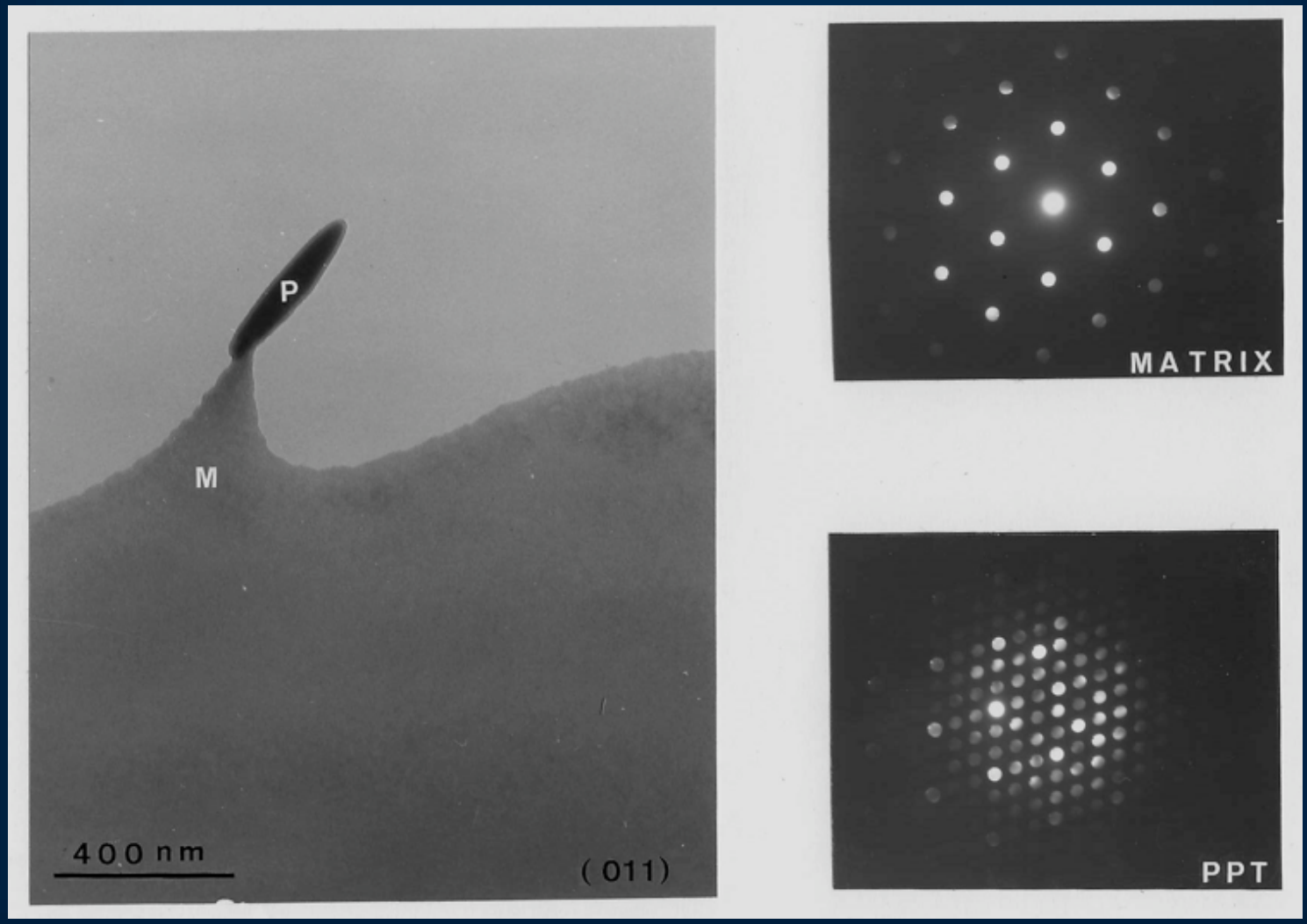

1. Diffraction pattern capability is one of the most important features of the TEM, because we can relate the crystallography to the images obtained.
2. The ability to determine crystallographic orientations locally (down to the nm level) gives the TEM its great advantage over the SEM and visible-light microscopes.
3. The questions that we can address using diffraction patterns obtained in the TEM include the following:
   - Is the specimen crystalline? Crystalline and amorphous materials have very different properties.
   - If it is crystalline, then what are the crystallographic characteristics (lattice parameter, symmetry, etc.) of the specimen?
   - Is the specimen monocrystalline? If not, what is the grain morphology, how large are the grains, what is the grain-size distribution, etc?
   - What is the orientation of the specimen or of individual grains with respect to the electron beam?
   - Is more than one phase present in the specimen?

Electron Beam Diffraction of a Pd film

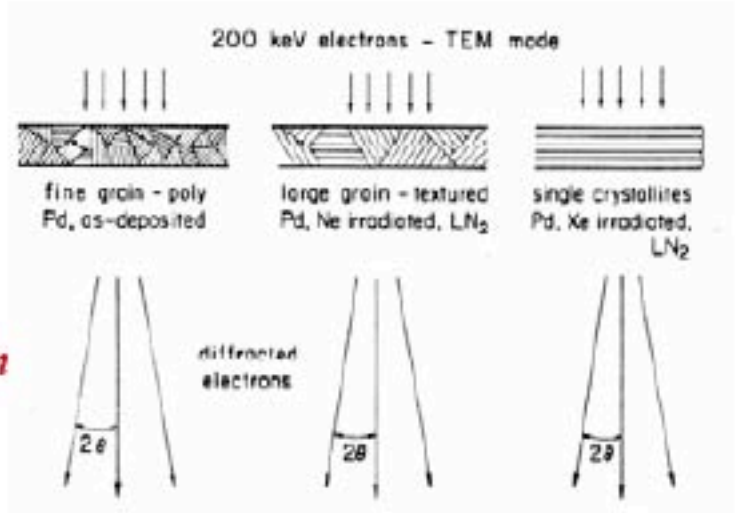

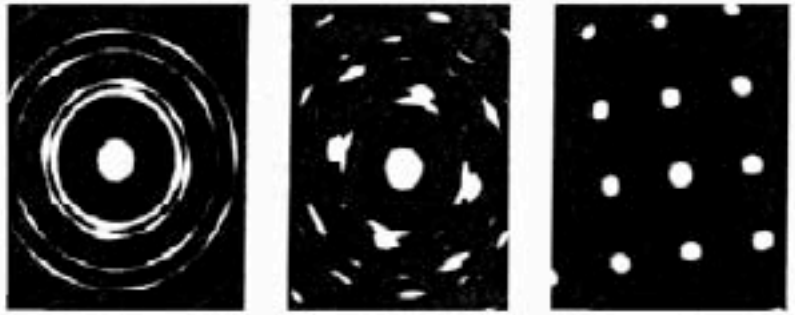

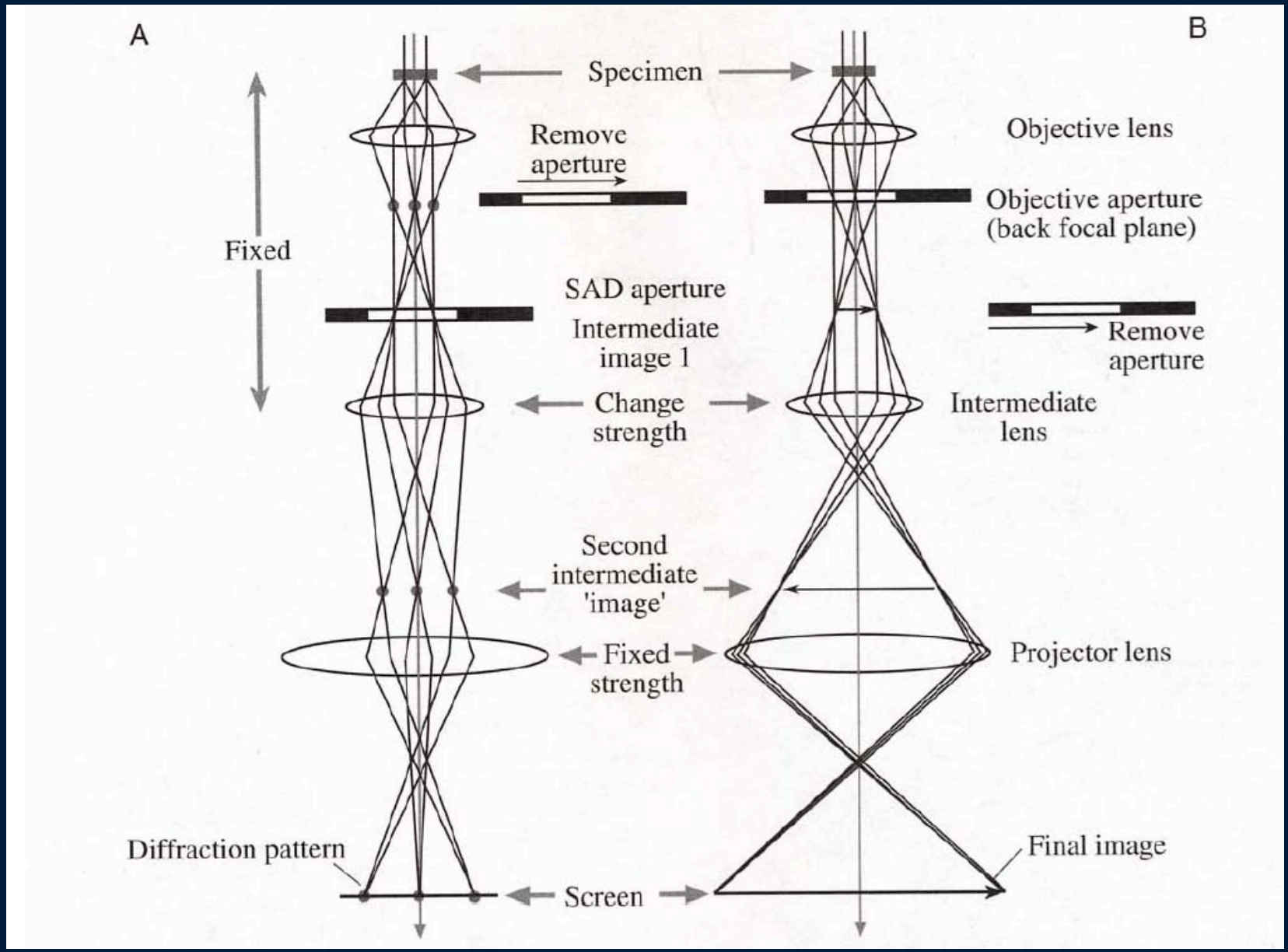
A
B
Specimen
Remove aperture
Objective lens
Objective aperture (back focal plane)
Fixed
SAD aperture
Intermediate image 1
Remove aperture
Change strength
Intermediate lens
Second intermediate 'image'
Fixed strength
Projector lens
Diffraction pattern
Screen
Final image

Type of Electron Scattering	Angular Range	Energy Loss
Unscattered	0	0
Elastic	10's-100's mR	~0
Phonon	10's-100's mR	<.025 eV
Inelastic	10's mR	everything else

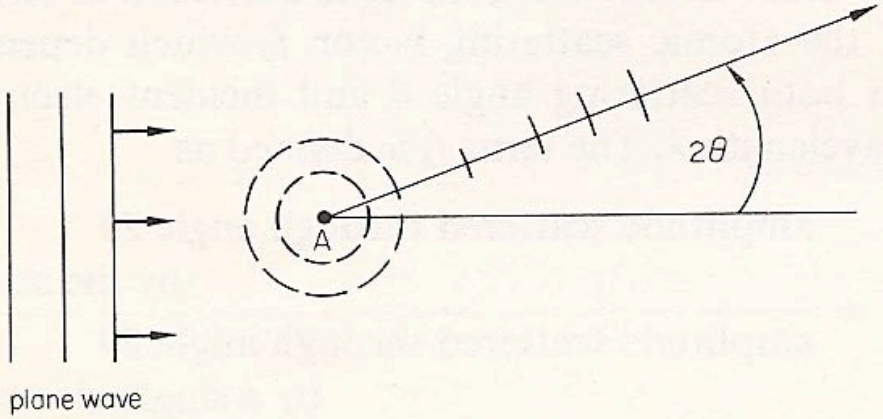

Figure 2.2 The scattering of a plane wave at an atom A through the formation of spherical wavelets travelling at an angle 2θ to the original direction of motion

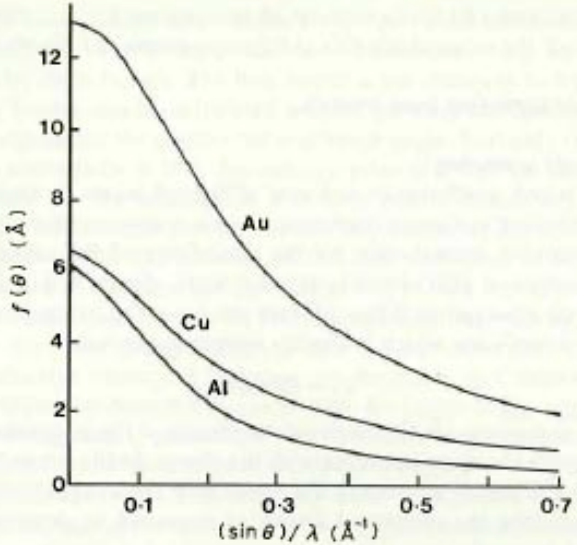

Fig. 2.2 Relationship between the atomic scattering factor $f(\theta)$ (in Å) and the scattering angle $(\sin\theta)/\lambda$ (in $Å^{-1}$) for aluminium, copper and gold calculated using equation (2.1).

Scattering from an isolated atom in free space

Elastic Scattering

Single Atoms:

$$I(\theta) \sim |f(\theta)|^2 = |f_o|^2 \bullet \frac{1}{(\theta^2 + \theta_o^2)^2}$$

$$\theta_o = \frac{1}{2\pi(0.885 a_o Z^{-1/3})}$$

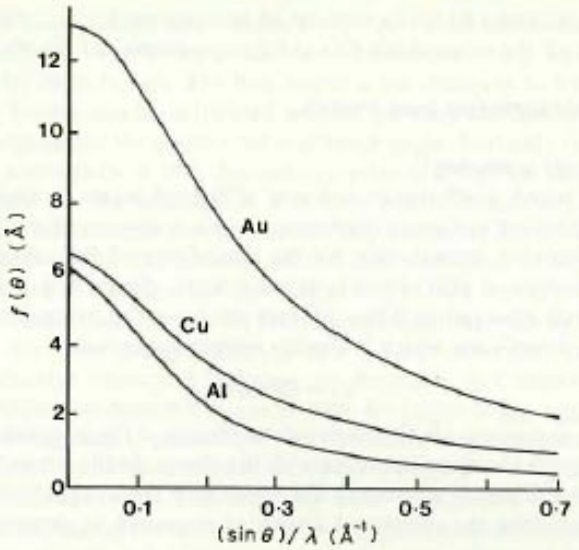

Fig. 2.2 Relationship between the atomic scattering factor $f(\theta)$ (in Å) and the scattering angle $(\sin\theta)/\lambda$ (in $Å^{-1}$) for aluminium, copper and gold calculated using equation (2.1).

Scattering from an collection of an amorphous collection of atoms
- neighboring atoms give rise to interference

Amorphous Solids:

$$I(\theta) \sim |f(\theta)|^2 \cdot \left\{1 + \frac{\sin(kR)}{kR}\right\}$$

$$k = \frac{4\pi}{\lambda}\sin(\theta)$$

R = Average Interatomic Spacing

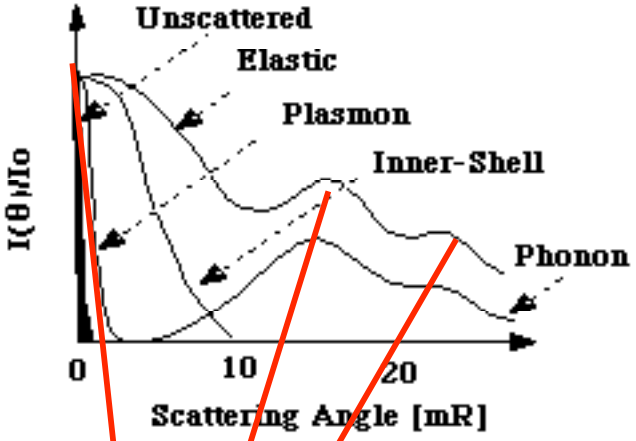

Amorphous Silica (SiO_2)

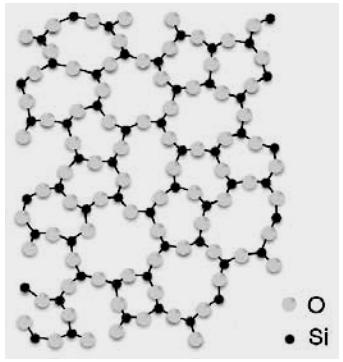

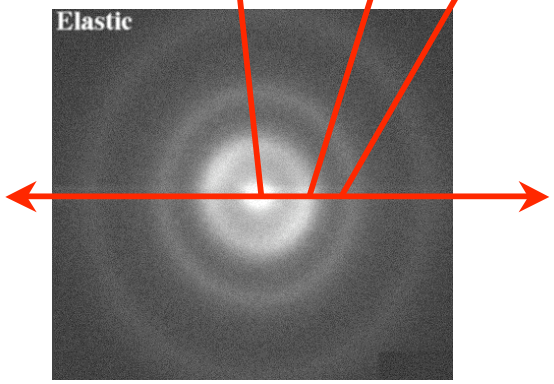

Solid State Order/DisOrder/Amorphization/ Studies

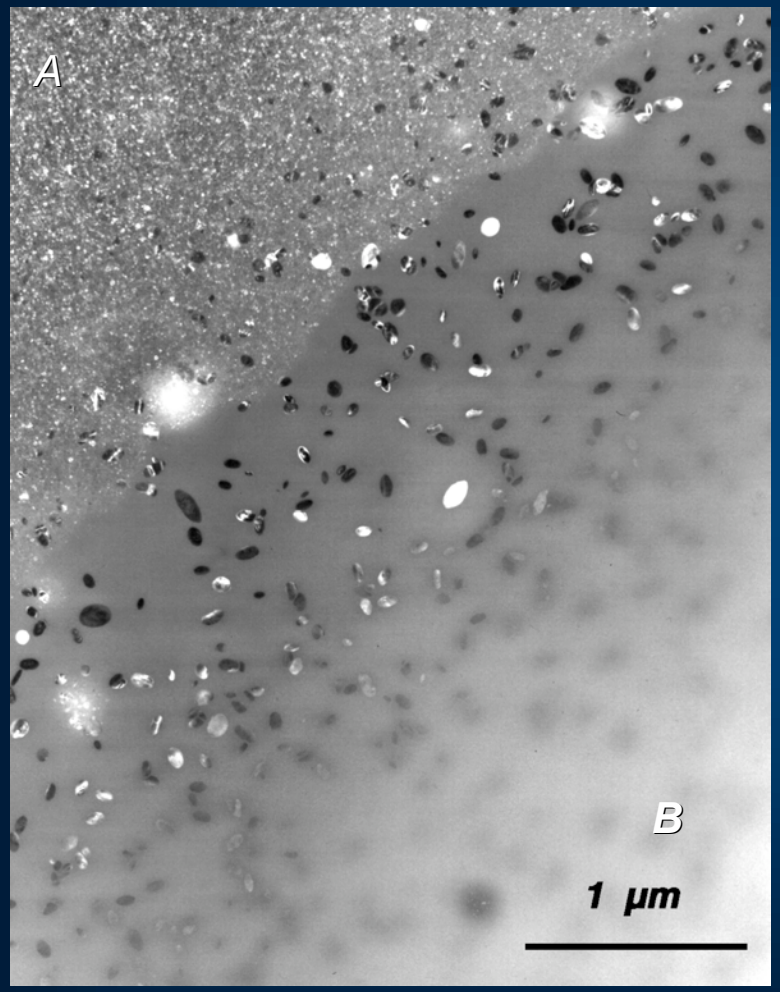

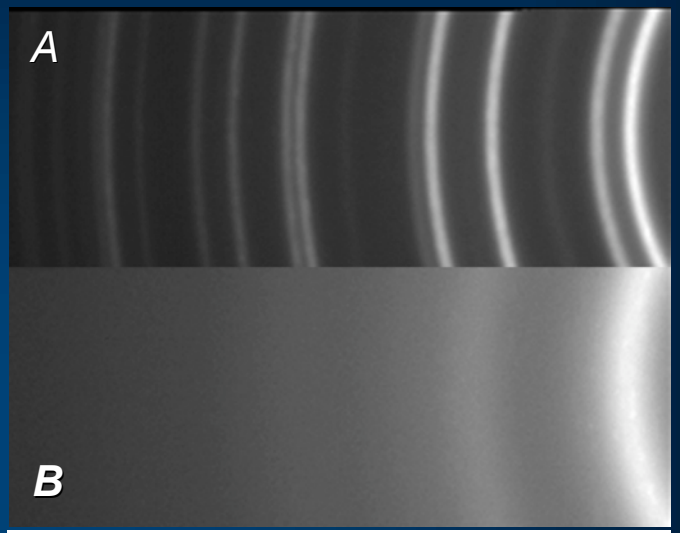

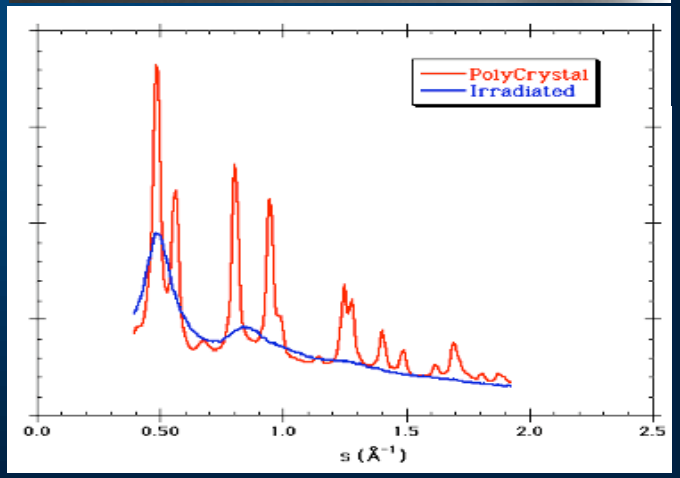

P.C. Liu, P. R. Okamoto,

Type of Electron Scattering	Angular Range	Energy Loss
Unscattered	0	0
Elastic	10's-100's mR	~0
Phonon	10's-100's mR	<.025 eV
Inelastic	10's mR	everything else

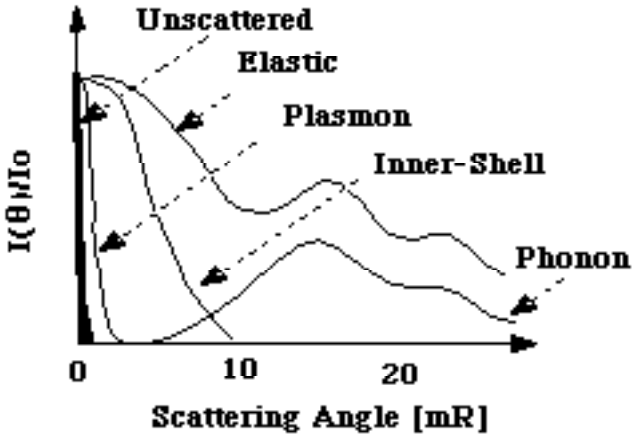

Amorphous Solids

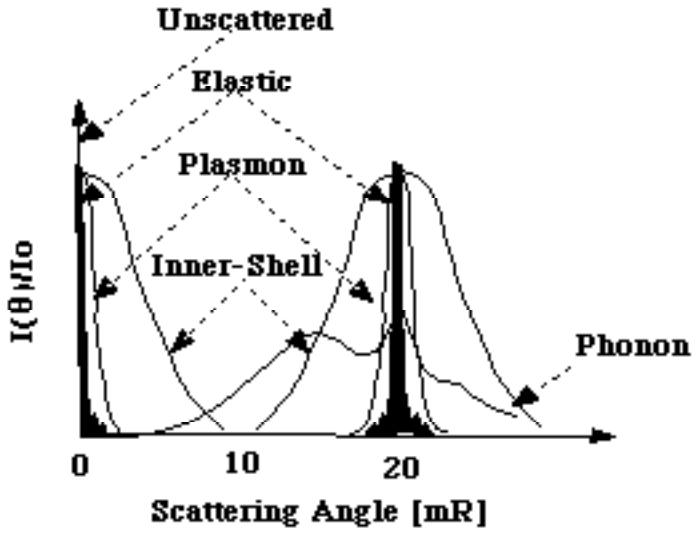

Crystalline Solids

14 Bravais Lattices in 7 Crystal Systems

Crystal system (Defining Symmetry)	Lattices:			
triclinic (none)	$\alpha, \beta, \gamma \neq 90°$			
monoclinic (1 diad)	simple $\alpha \neq 90°$ $\beta, \gamma = 90°$	base-centered $\alpha \neq 90°$ $\beta, \gamma = 90°$		
orthorhombic (3 perpendicular diads)	simple $a \neq b \neq c$	base-centered $a \neq b \neq c$	body-centered $a \neq b \neq c$	face-centered $a \neq b \neq c$
hexagonal (1 hexad)	$a \neq c$			
rhombohedral (1 triad)	$\alpha, \beta, \gamma \neq 90°$			
tetragonal (1 tetrad)	simple $a \neq c$	body-centered $a \neq c$		
cubic (4 triads)	simple	body-centered	face-centered	

Seven Crystal Systems

Crystal system		Interplanar spacing of the (hkl) plane
cubic	$a = b = c$ $\alpha = \beta = \gamma = 90°$	$\frac{1}{d^2} = \frac{1}{a^2}(h^2 + k^2 + l^2)$
tetragonal	$a = b \neq c$ $\alpha = \beta = \gamma = 90°$	$\frac{1}{d^2} = \frac{1}{a^2}(h^2 + k^2) + \frac{1}{c^2}l^2$
orthorhombic	$a \neq b \neq c$ $\alpha = \beta = \gamma = 90°$	$\frac{1}{d^2} = \frac{1}{a^2}h^2 + \frac{1}{b^2}k^2 + \frac{1}{c^2}l^2$
hexagonal	$a = b \neq c$ $\alpha = \beta = 90°; \gamma = 120°$	$\frac{1}{d^2} = \frac{4}{3a^2}(h^2 + hk + k^2) + \frac{1}{c^2}l^2$
rhombohedral	$a = b = c$ $\alpha = \beta = \gamma < 120° \neq 90°$	$\frac{1}{d^2} = \frac{1}{a^2}\frac{(1 + \cos\alpha)\{(h^2 + k^2 + l^2) - (1 - \tan^2\frac{1}{2}\alpha)(hk + kl + lh)\}}{1 + \cos\alpha - 2\cos^2\alpha}$
monoclinic	$a \neq b \neq c$ $\alpha = \gamma = 90° \neq \beta$	$\frac{1}{d^2} = \frac{1}{a^2}\frac{h^2}{\sin^2\beta} + \frac{1}{b^2}k^2 + \frac{1}{c^2}\frac{l^2}{\sin^2\beta} - \frac{2hl\cos\beta}{ac\sin^2\beta}$
triclinic	$a \neq b \neq c$ $\alpha \neq \beta \neq \gamma$	$\frac{1}{d^2} = \frac{1}{V^2}(s_{11}h^2 + s_{22}k^2 + s_{33}l^2 + 2s_{12}hk + 2s_{23}kl + 2s_{33}lh)$ where $V^2 = a^2b^2c^2(1 - \cos^2\alpha - \cos^2\beta - \cos^2\gamma + 2\cos\alpha\cos\beta\cos\gamma)$ and $s_{11} = b^2c^2\sin^2\alpha$ $s_{22} = a^2c^2\sin^2\beta$ $s_{33} = a^2b^2\sin^2\gamma$ $s_{12} = abc^2(\cos\alpha\cos\beta - \cos\gamma)$ $s_{23} = a^2bc(\cos\beta\cos\gamma - \cos\alpha)$ $s_{31} = ab^2c(\cos\gamma\cos\alpha - \cos\beta)$

Periodic Structures
Create Constructive/Destructive Interference

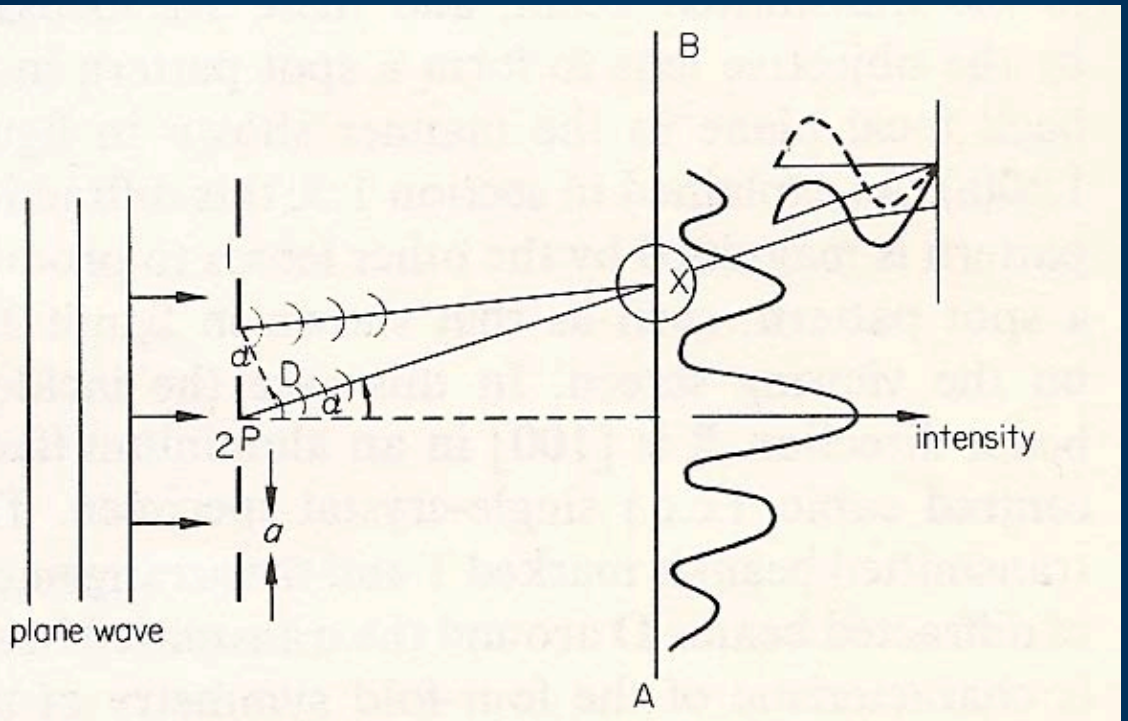

Figure 2.4 Diffraction of monochromatic light by a line grating. Inset shows waves arriving at X in phase

Simple Geometrical Description of Bragg's Law

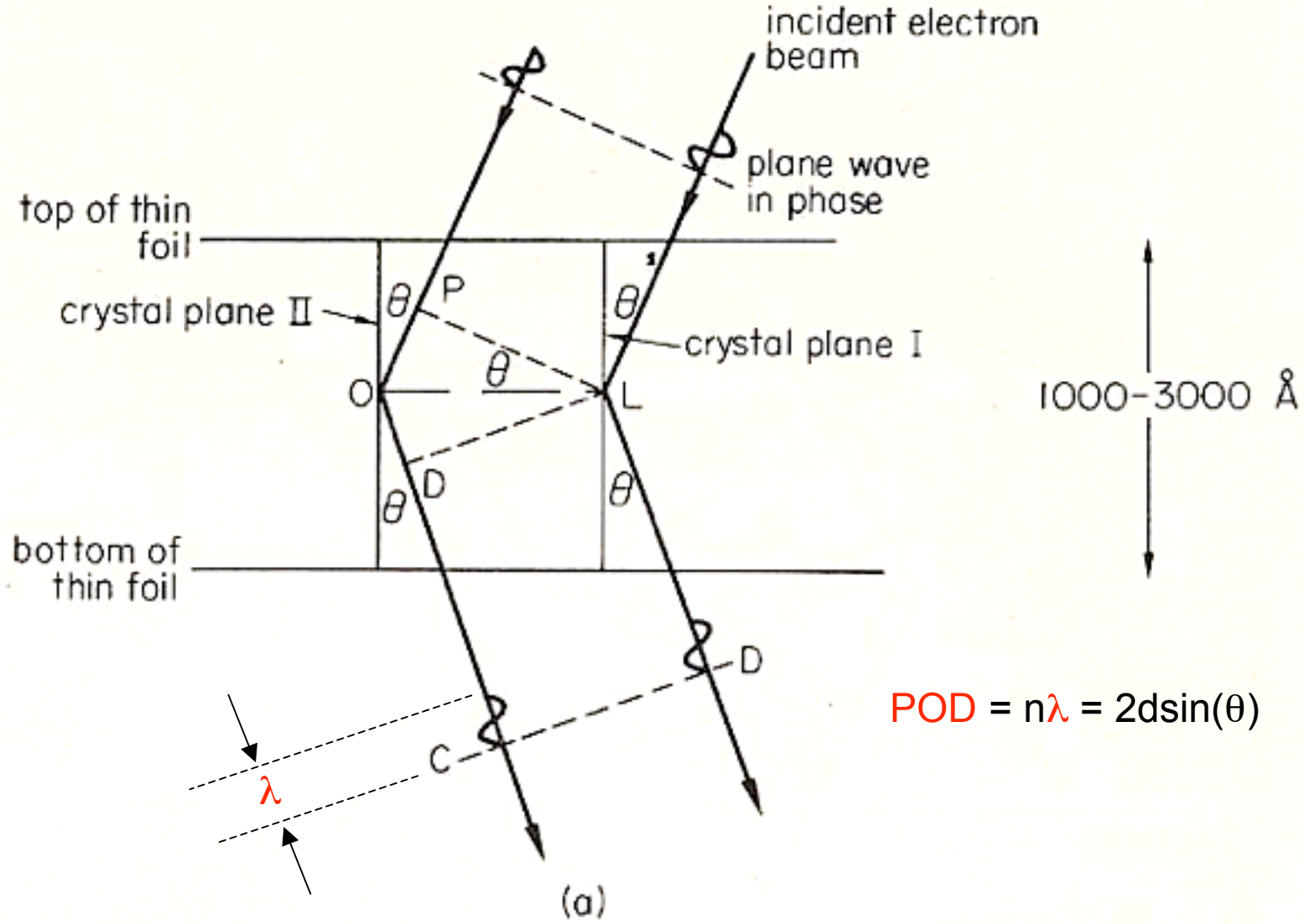

$POD = n\lambda = 2d\sin(\theta)$

Elastic Scattering

Crystalline Solids:

$$I(\theta) \sim |F(hkl)|^2$$

$$F(hkl) = \sum_j f_j(\theta)\, e^{(-2\pi i \vec{k}\cdot\vec{r})}$$

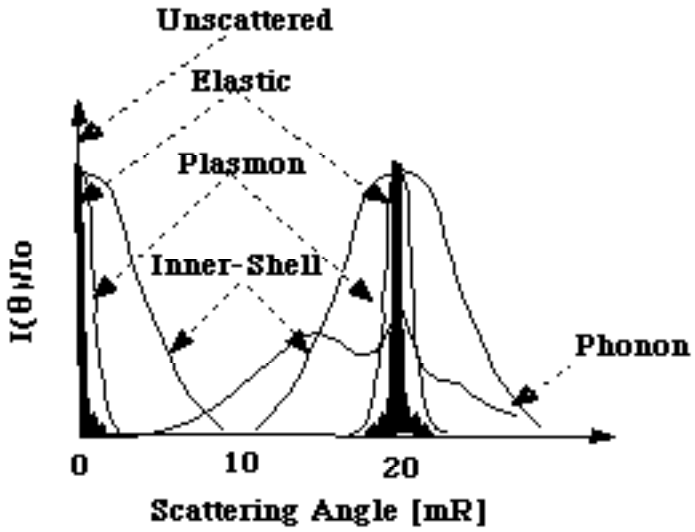

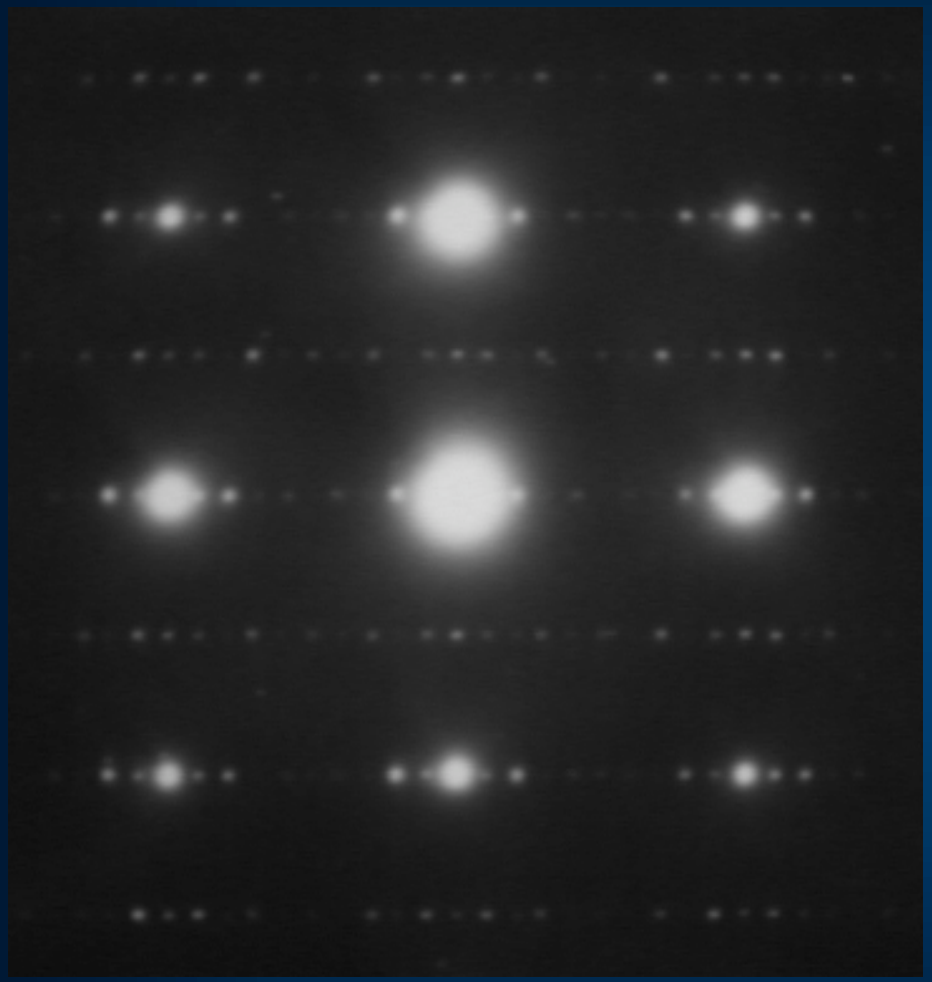

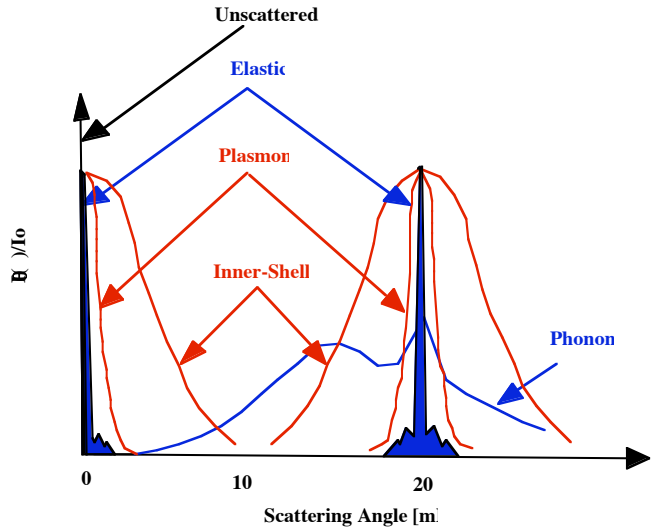

Elastic Scattering : Crystalline Solids

$$I(\theta) \sim |F(hkl)|^2$$

$$F(hkl) = \sum_j f_j(\theta) \exp\left(-2\pi i \vec{g} \cdot \vec{r}\right)$$

$$V(r) = -\sum_g^{?} V_g \exp\left(2\pi i \bar{g}.\bar{r}\right) \quad ; \quad V_g = \frac{h^2}{2\pi m V_e} f(\theta)$$

Type of Diffraction Patterns

- Electron diffraction patterns produced in transmission in the electron microscope can be of three different types.
  - (a) Ring pattern — Polycrystalline, and amorphous specimen
  - (b) Spot pattern — Single-crystal region of the specimen
  - (c) Kikuchi line pattern

- Type (b) and (c) often occur on the same diffraction pattern. In general, spot and Kikuchi patterns will be taken from a specific area of the specimen and are known as ‘selected area’ diffraction patterns (SADPs).

Ring Pattern:

- The major use of ring patterns is in the identification of phases using extraction replicas. These diffraction patterns also arise from very fine grain size polycrystalline material such as physically or chemically vapor deposited or electrodeposited thin foils.

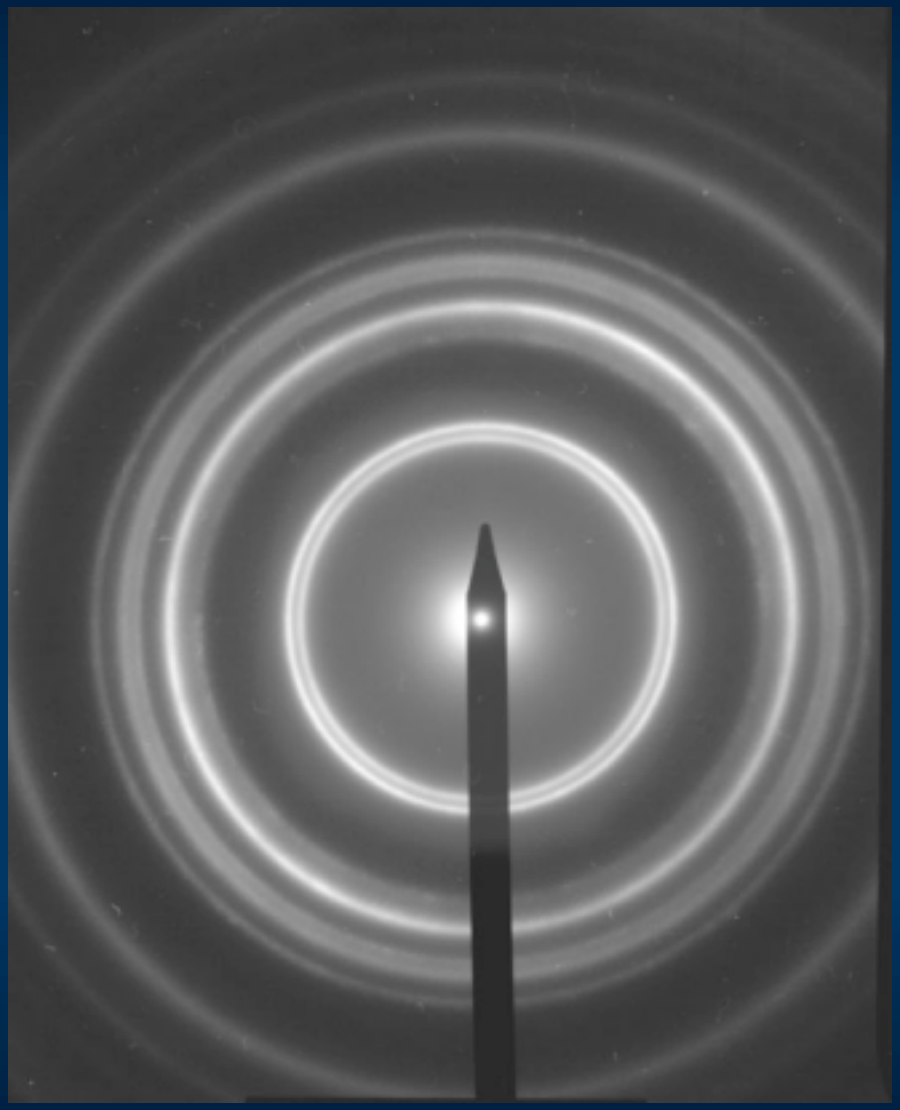

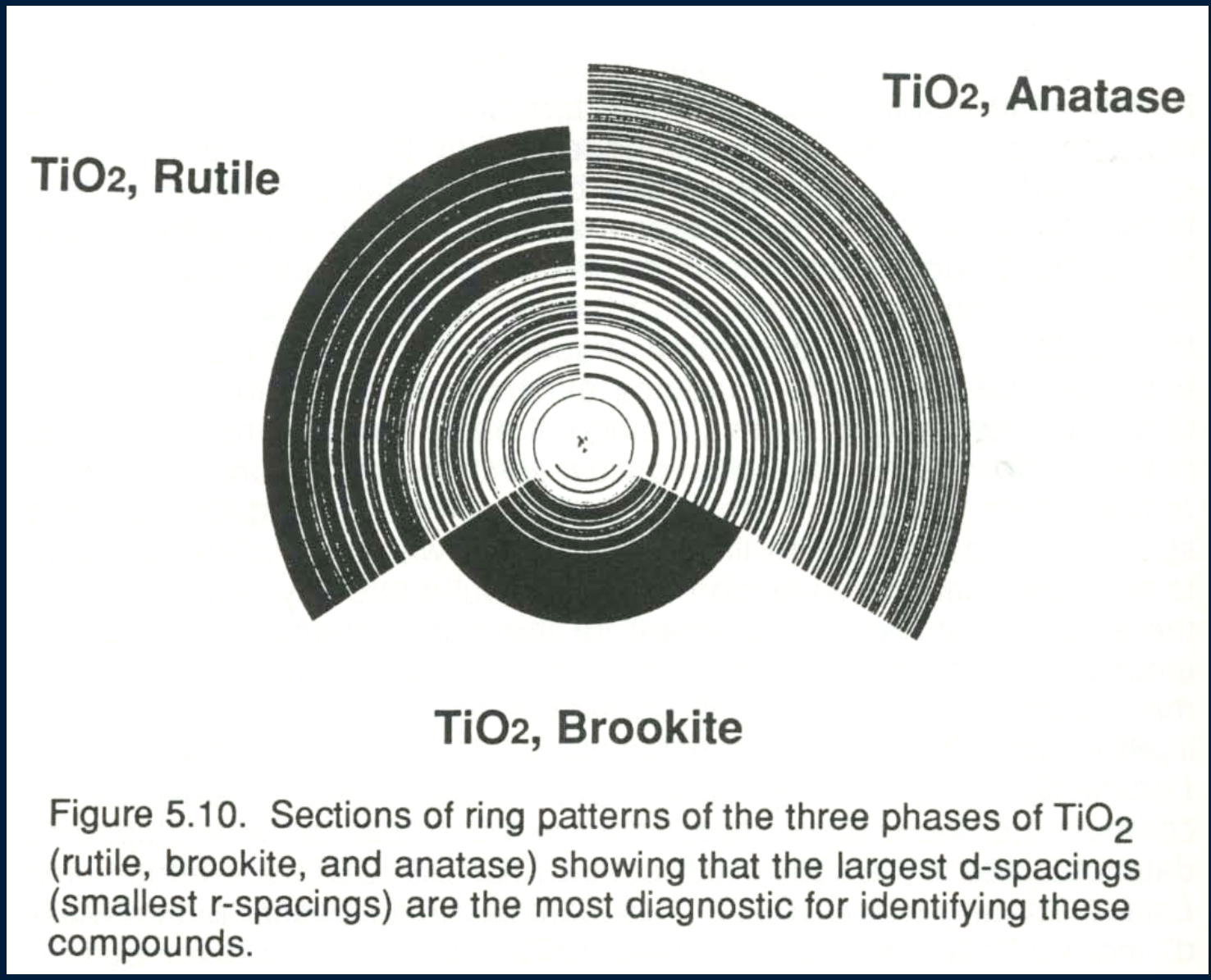

Figure 5.10. Sections of ring patterns of the three phases of TiO_2 (rutile, brookite, and anatase) showing that the largest d-spacings (smallest r-spacings) are the most diagnostic for identifying these compounds.

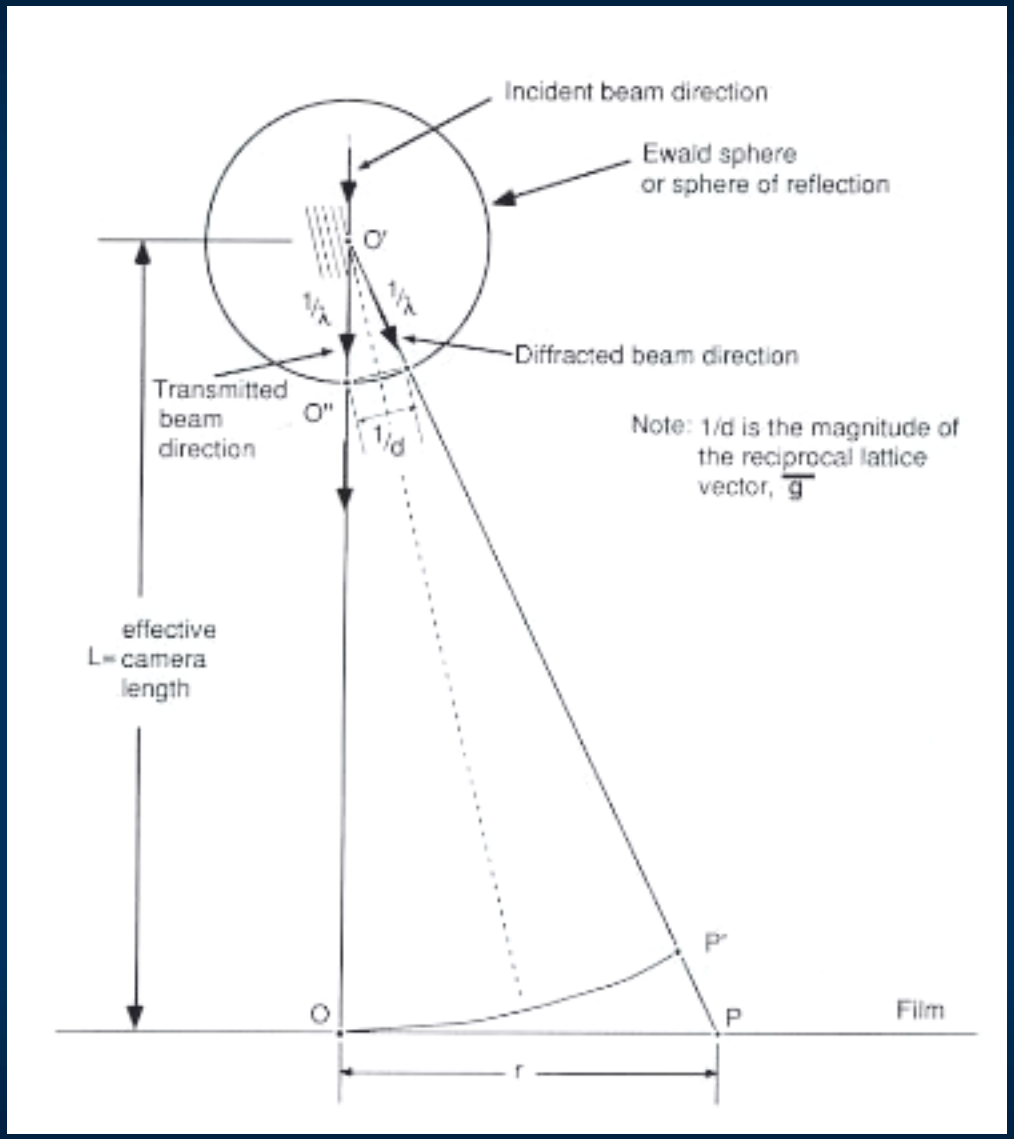
Incident beam direction
Ewald sphere
or sphere of reflection
O'
1/λ
1/λ
Diffracted beam direction
Transmitted
beam
direction
O"
1/d
Note: 1/d is the magnitude of
the reciprocal lattice
vector, g
effective
L= camera
length
P'
O
P
Film
r

Ring pattern: what can we obtain

- d-spacing

$$Rd_{hkl} = L\lambda$$

R: the measured ring radius

d_{hkl}: the d-spacing being measured

L: camera length

λ: wave length of electron beam

- Camera length calibration
- Crystalline / particle fineness

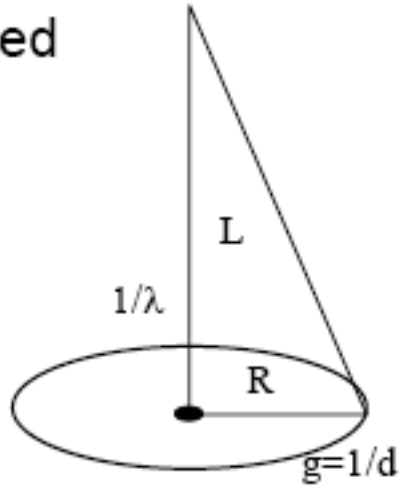

$$Rd_{hkl} = \lambda L$$

$$\lambda_{rel} = \frac{h}{mv} = \frac{h}{m_0 v}\sqrt{1-\gamma^2}$$

$$= \frac{12.27}{\sqrt{V_a}}\left[1 + 0.978 \times 10^{-6} V_a\right]^{-1/2}$$

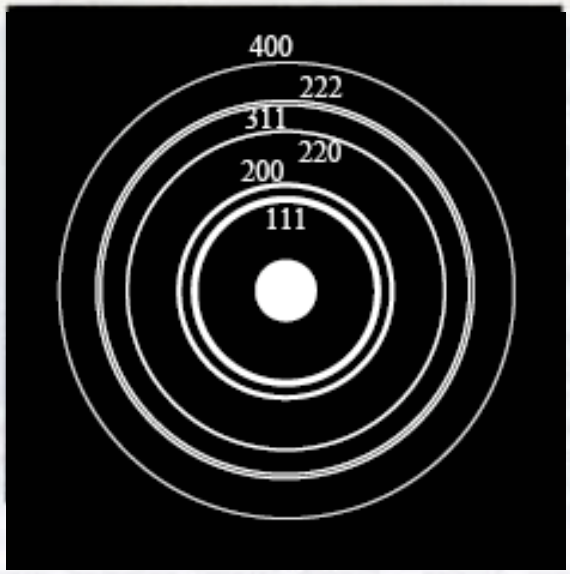

Use the cubic interplanar spacing formula

$$d_{hkl} = \frac{a}{\sqrt{h^2+k^2+l^2}}, \quad a = 0.40497 \text{ nm}$$

to calculate the d-spacings below for the first five reflections of aluminum:

r-distance	hkl	d-spacing	λL
10.3 mm	111	0.2338 nm	2.408 nm-mm
11.9	200	0.2025	2.409
16.8	220	0.1432	2.406
19.7	311	0.1221	2.405
20.6	222	0.1169	2.408
		Average =	2.407 nm-mm

Electron Properties as a Function of Accelerating Voltage

Table 1.2. Electron Properties as a Function of Accelerating Voltage

Accelerating voltage (kV)	Nonrelativistic wavelength (nm)	Relativistic wavelength (nm)	Mass ($\times m_0$)	Velocity ($\times 10^8$ m/s)
100	0.00386	0.00370	1.196	1.644
120	0.00352	0.00335	1.235	1.759
200	0.00273	0.00251	1.391	2.086
300	0.00223	0.00197	1.587	2.330
400	0.00193	0.00164	1.783	2.484
1000	0.00122	0.00087	2.957	2.823

Electron Beam Diffraction of a Pd film

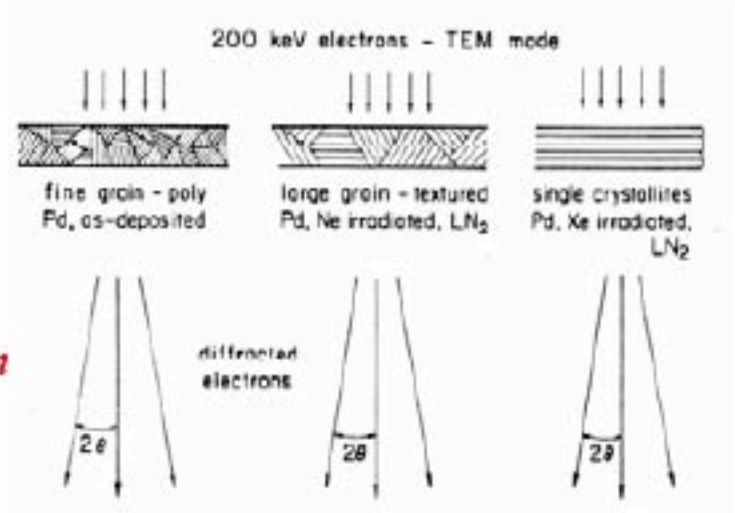

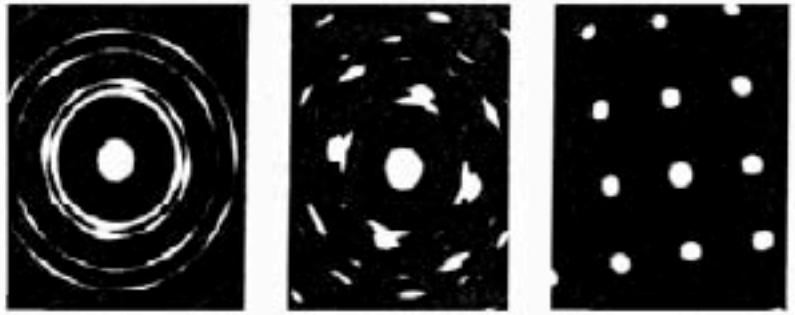

Indexing Diffraction patterns

The Ring Patterns

The radius of each ring is characteristic of the spacing of the reflecting planes in the crystal and the magnification settings of the microscope lenses.

Procedure for indexing ring patterns is as follows:

1. When the identity of the material is known, we have the following:
    - Measure the ring diameters.
    - Determine the ratios of the squares of the diameters of the outer rings to that of the first or second (low-index) ring.
    - Check the ratios against a table of ratios of the interplanar spacings for the crystal structure of interest, see table 2.2.
2. When the identity of the substance is unknown, we have the following:
    - Measure the diameter of the rings.
    - Convert the distances into interplanar spacings using the camera constant defined as $Rd = \lambda L$.
    - Use ASTM (American Society for Testing Materials) index to identify the phase, starting with the most likely on the basis of the known constituents of the alloy.

Diffraction patterns from polycrystalline specimens are most commonly used either to calibrate the camera length or to identify precipitates.

Table 2.2 Proportionalities of the ratios of the radii of ring patterns for different crystal structures

Crystal structure	Formula for interplanar spacing	Possible values of h, k, l for reflection (up to 20)	Criterion
simple cubic	$\frac{1}{d^2} = \frac{h^2 + k^2 + l^2}{a^2} = \frac{N}{a^2}$	N an integer except 7 or 15	ratios of squares of radii $\propto N$
f.c.c.	$\frac{1}{d^2} = \frac{h^2 + k^2 + l^2}{a^2} = \frac{N}{a^2}$	$N = 3, 4, 8, 11, 12, 16, 19, 20$	ratios $\propto N$
b.c.c.	$\frac{1}{d^2} = \frac{h^2 + k^2 + l^2}{a^2} = \frac{N}{a^2}$	$N = 2, 4, 6, 8, 10, 12, 14, 16, 18, 20$	ratios $\propto N$
diamond structure	$\frac{1}{d^2} = \frac{h^2 + k^2 + l^2}{a^2} = \frac{N}{a^2}$	$N = 2, 8, 11, 16, 19$	ratios $\propto N$
tetragonal	$\frac{1}{d^2} = \frac{h^2 + k^2}{a^2} + \frac{l^2}{c^2}$	$h^2 + k^2 = 1, 2, 4, 5, 8, 9, 10, 13, 16, 17, 18, 20$	ratios frequently proportional to 2; use Bunn chart, see Henry *et al.* (1951)
hexagonal	$\frac{1}{d^2} = \frac{4}{3}\frac{h^2 + hk + k^2}{a^2} + \frac{l^2}{c^2}$	$h^2 + hk + l^2 = 1, 3, 4, 7, 9, 12, 13, 16, 19$	ratios frequently proportional to 3; use Bunn chart, see Henry *et al.* (1951)

Table A4.1 Occurrence of reflections for the cubic crystal structures

Line no. $N = h^2+k^2+l^2$	hkl indices	$N^{1/2} = (h^2 + k^2 + l^2)^{1/2}$	b.c.c.	f.c.c.	diamond	Line no. $N = h^2+k^2+l^2$	hkl indices	$N^{1/2} = (h^2 + k^2 + l^2)^{1/2}$	b.c.c.	f.c.c.	diamond
1	100	1.00				33	522, 441	5.745			
2	110	1.414	×			34	530, 433	5.831	×		
3	111	1.732		×	×	35	531	5.916		×	×
4	200	2.00	×	×	×	36	600, 442	6.00	×	×	×
5	210	2.236				37	610	6.083			
6	211	2.450	×			38	611, 532	6.164	×		
7	—	—				39	—	—			
8	220	2.828	×	×	×	40	620	6.325	×	×	×
9	300, 221	3.00				41	621, 540, 443	6.403			
10	310	3.162	×			42	541	6.481	×		
11	311	3.317		×	×	43	533	6.557		×	×
12	222	3.464	×	×		44	622	6.633	×	×	×
13	320	3.606				45	630, 542	6.708			
14	321	3.742	×			46	631	6.782	×		
15	—	—				47	—	—			
16	400	4.00	×	×	×	48	444	6.928	×	×	
17	410, 322	4.123				49	700, 632	7.00			
18	411, 330	4.243	×			50	710, 550, 543	7.071	×		
19	331	4.359		×	×	51	711, 551	7.141		×	×
20	420	4.472	×	×	×	52	640	7.211	×	×	
21	421	4.583				53	720, 641	7.280			
22	332	4.690	×			54	721, 633, 552	7.349	×		
23	—	—				55	—	—			
24	422	4.899	×	×	×	56	642	7.483	×	×	×
25	500, 430	5.00				57	722, 544	7.550			
26	510, 431	5.099	×			58	730	7.616	×		
27	511, 333	5.196		×	×	59	731, 553	7.681		×	×
28	—	—				60	—	—			
29	520, 432	5.385				61	650, 643	7.810			
30	521	5.477	×			62	732, 651	7.874	×		
31	—	—				63	—	—			
32	440	5.657	×	×	×	64	800	8.00	×	×	×

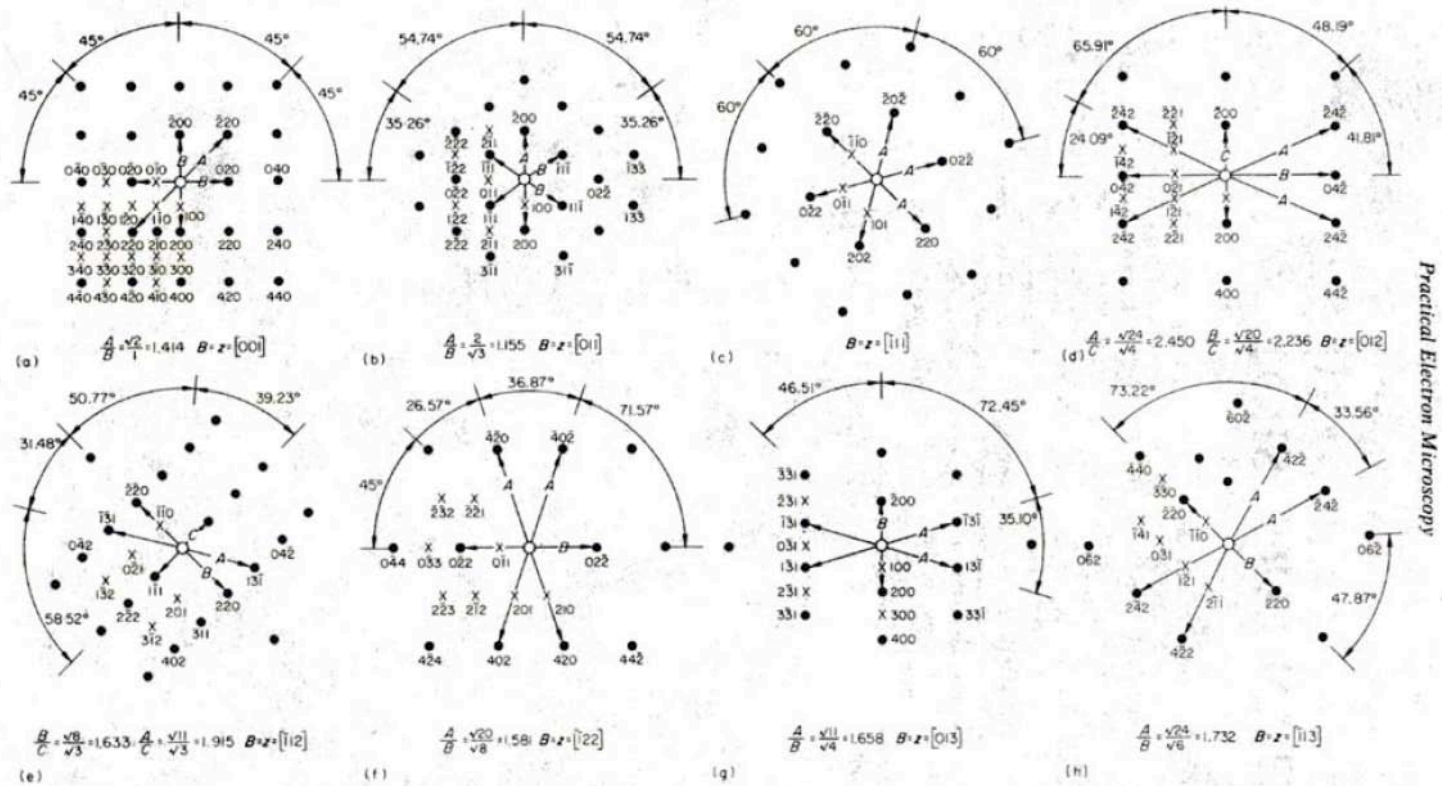

Figure A4.1 Single-crystal spot transmission electron diffraction patterns for the f.c.c. crystal structure ($u^2 + v^2 + w^2 < 22$). The zone axis z, defined in appendix 1, is the beam direction B defined in section 2.7.2, as indicated. The crosses in one quadrant of the diagram indicate the positions of the spots for the ordered f.c.c. ($L1_2$) unit cell. The complete pattern may be generated by repeating these spots in the remainder of the pattern and indexing using the addition of vectors, see section 2.7.2.1

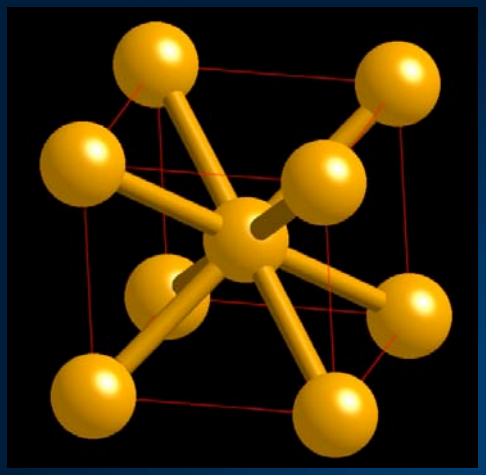

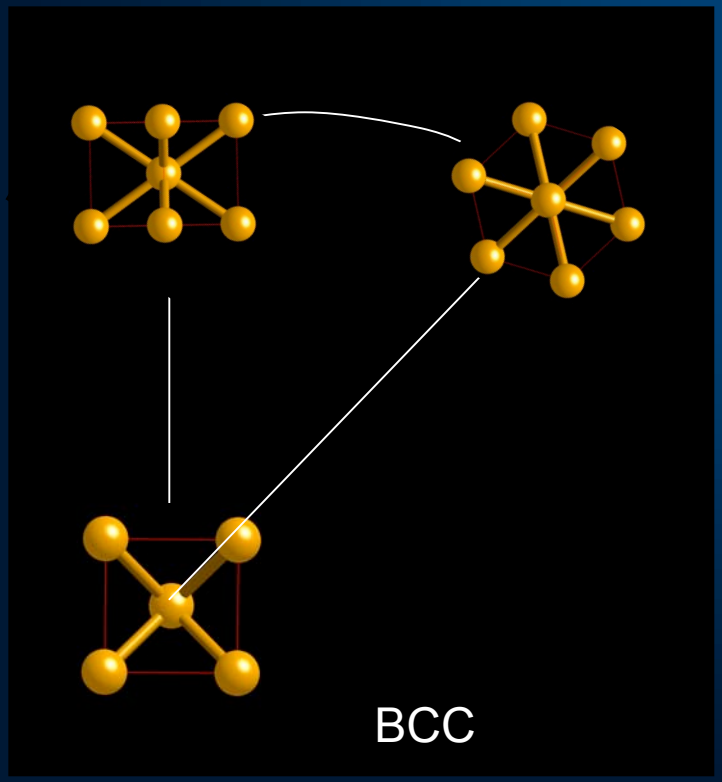

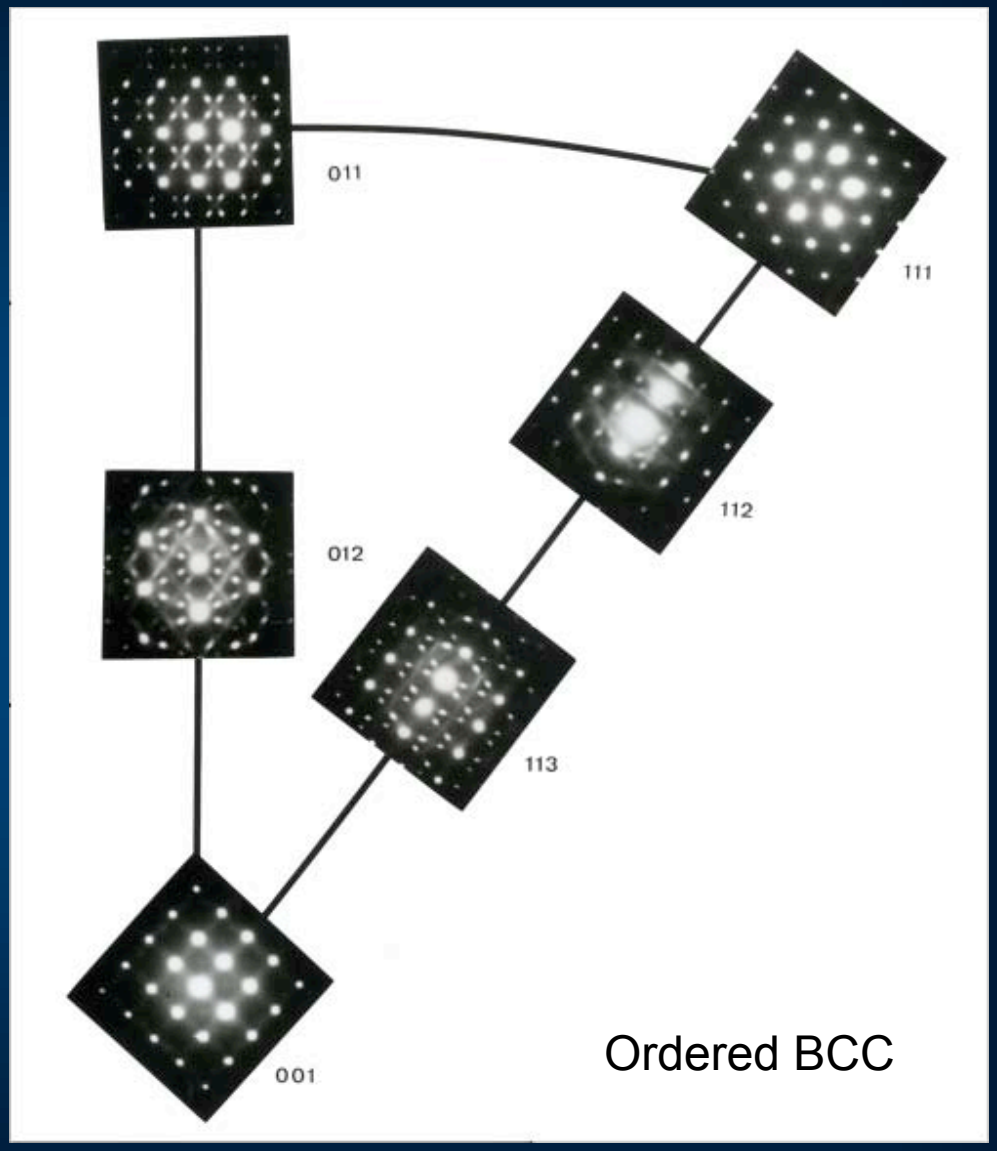

Diffraction Space is related to Real Space

Index Simple Patterns – spots are produced by planes in one zone

- Frequently these patterns may be easily recognized from their simplicity and their six-, four-, three- and two-fold symmetry.

(a) *Indexing the pattern*. The indexing procedure involves one of two procedures:

(i) Camera constant method –Camera constant known, materials known. Measure the distance R of the spot from the center spot, figure 2.20 (a) (most accurately determined by measuring the total distance between several spots in this direction and dividing as necessary). Divide the camera constant λL ($Rd = \lambda L$) by R and check the result against a list of d spacings.

(ii) Method of ratios. Camera constant unknown. Material λL known. Measure distances of spots from center spot relative to that between the nearest spot and the center. Check against tables of ratios of d spacings for low-index planes. Account must be taken of the occurrence of planes with the same d spacing, see table A 4.1.

Kikuchi Lines

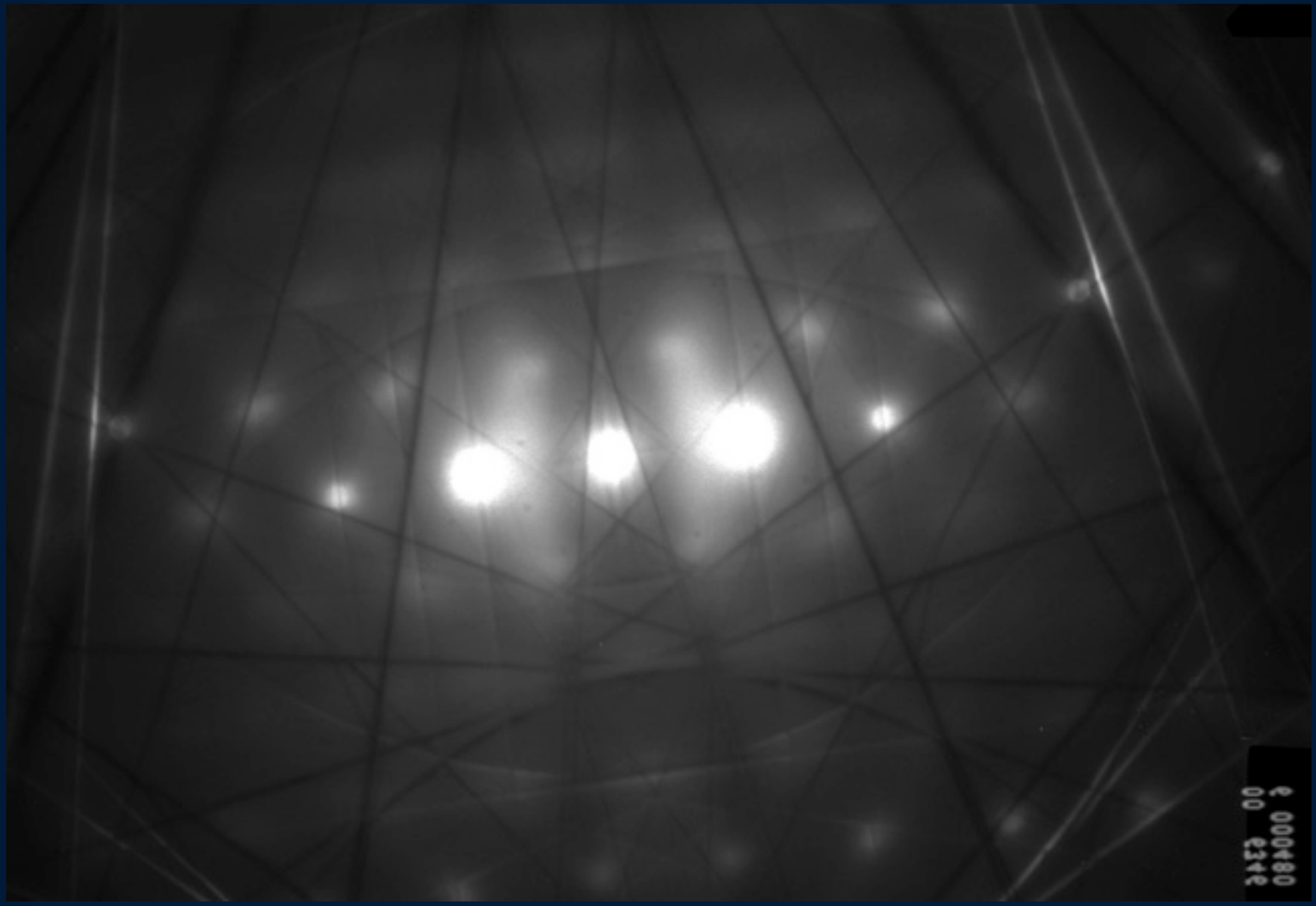

Kikuchi Lines

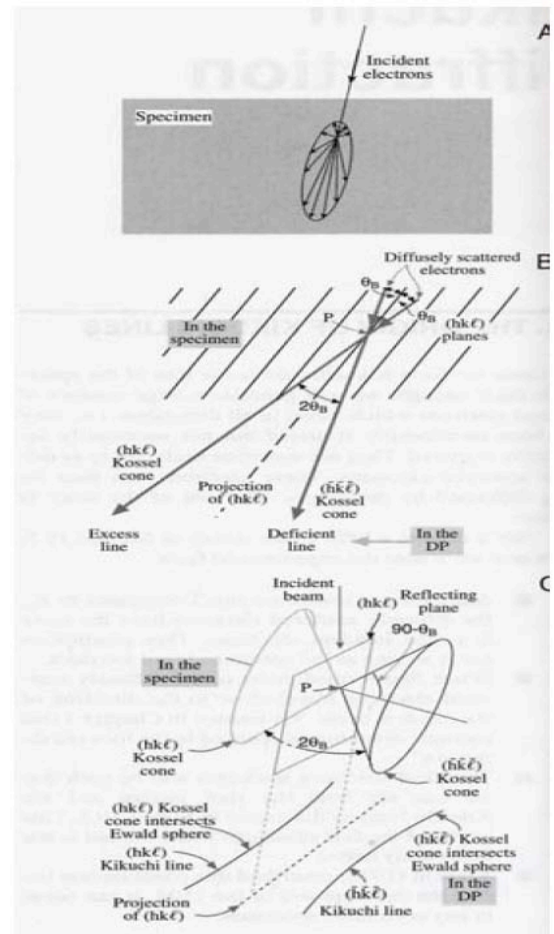

Figure 19.2. (A) Schematic representation of all electron scatter
calized at a single point in the specimen. In (B) some of the scattere
trons are diffracted because they travel at the Bragg angles θ_B to
$hk\ell$ planes. The diffracted electrons form Kossel cones centered a
the diffracting planes. The lines closest to the incident beam directi
dark (deficient) and the lines furthest away from the beam are brig
cess). In (C) the cones intercept the Ewald sphere, creating par
which approximate to straight Kikuchi lines in the diffraction patte
cause θ_B is small.

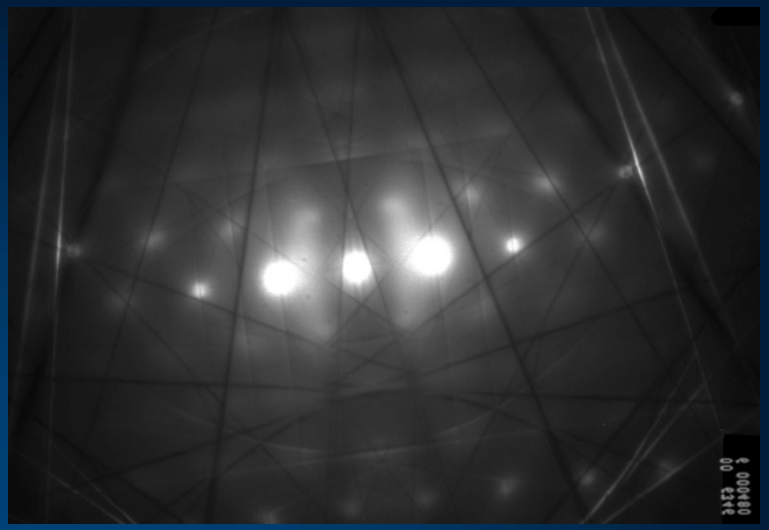

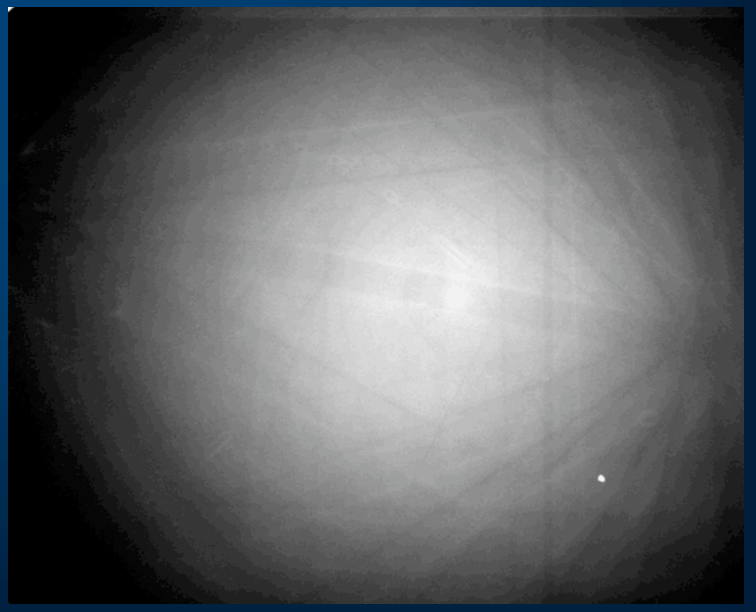

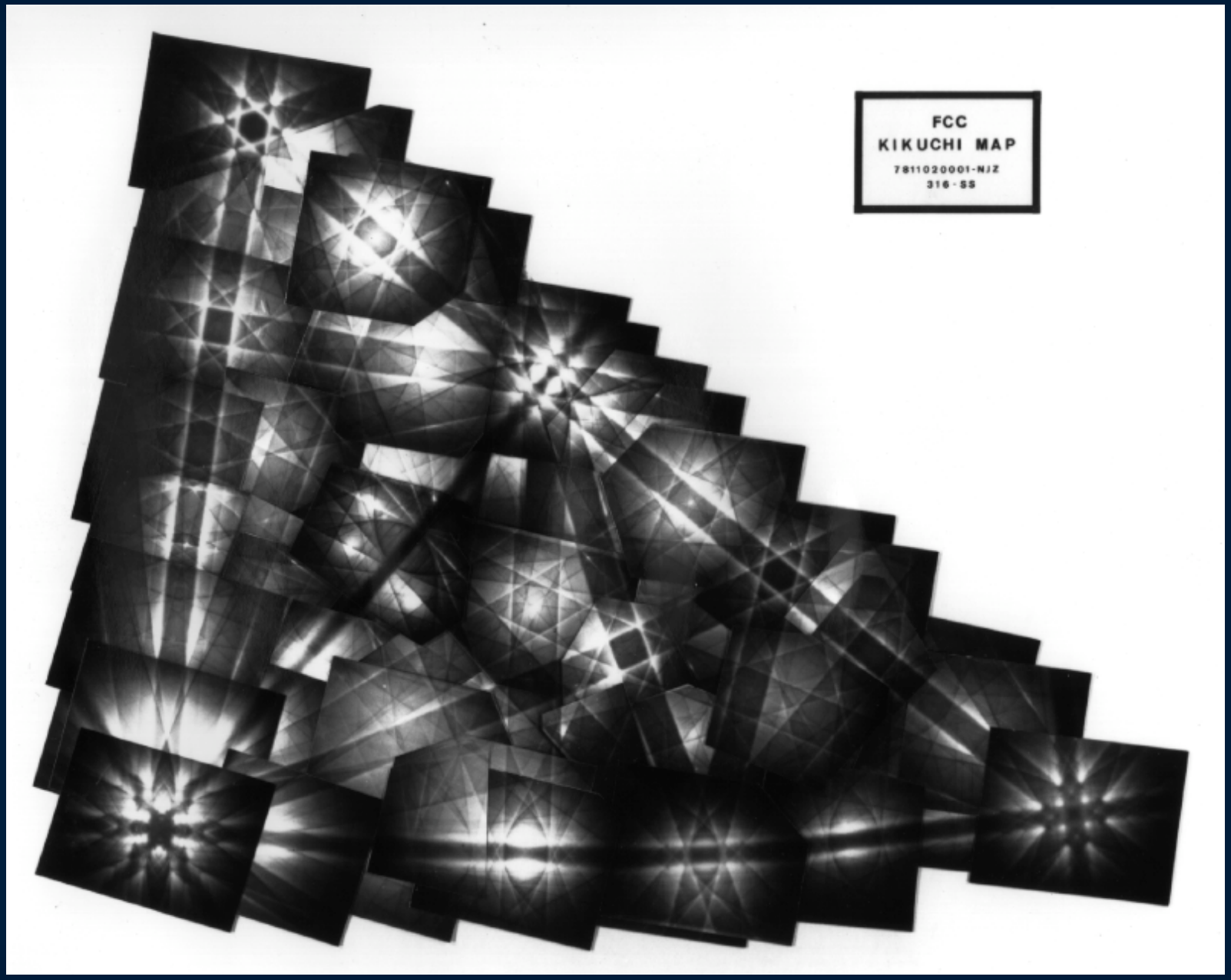
FCC
KIKUCHI MAP
7811020001-NJZ
316-SS

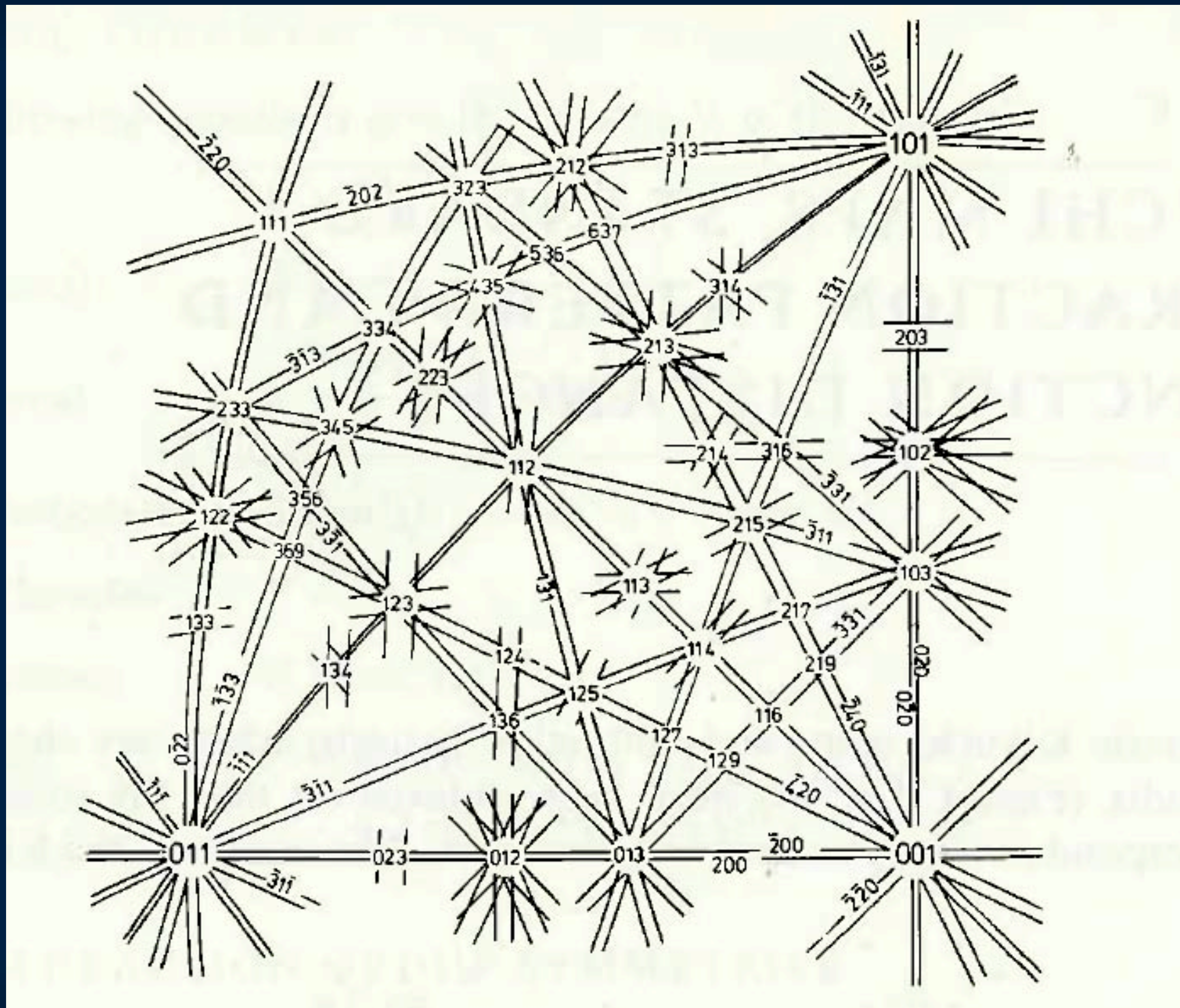
101
111
131
313
212
323
202
220
111
637
536
435
314
131
203
334
213
223
313
233
345
112
214
316
102
356
331
122
215
311
369
103
123
113
131
217
133
331
114
124
134
219
133
125
020
116
136
127
240
022
111
129
311
220
011
023
012
013
200
200
001
311
220

Specimen Holders

Single-titl holder
Double-tilt holder
Low-background holder
Heating holder
Cooling holder
Cryo-transfer holder

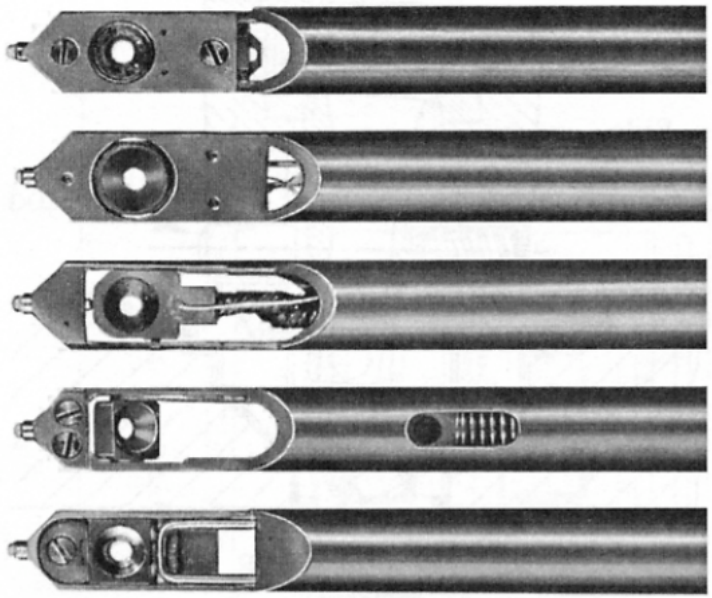

Figure 8.8. Examples of different designs for the side-entry holder. From the top, they are: a rotation holder, a heating holder, a cooling holder, a double-tilt holder, and a single-tilt holder.

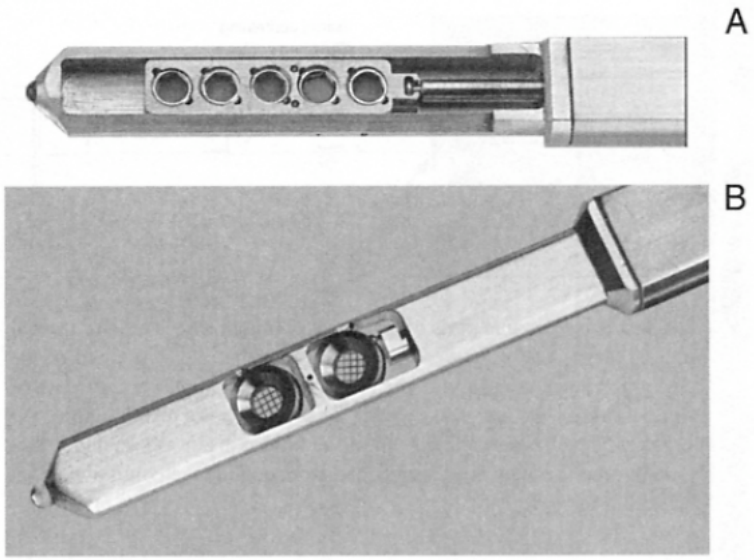

Figure 8.9. Multiple-specimen holders. (A) Five-specimen single-tilt and (B) two-specimen double-tilt.

How do Apertures & Condensor Lens affect Diffraction

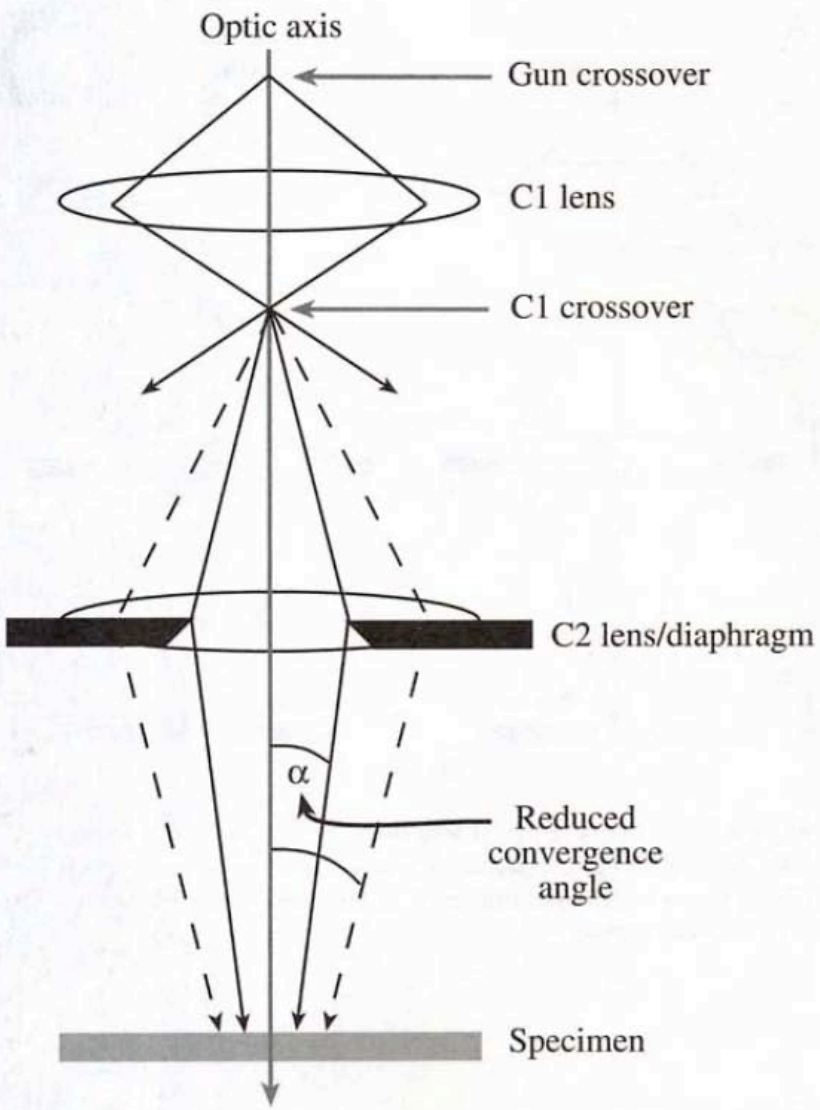

Figure 9.2. Effect of the C2 aperture on the beam coherence: a smaller aperture creates a more parallel, more coherent beam.

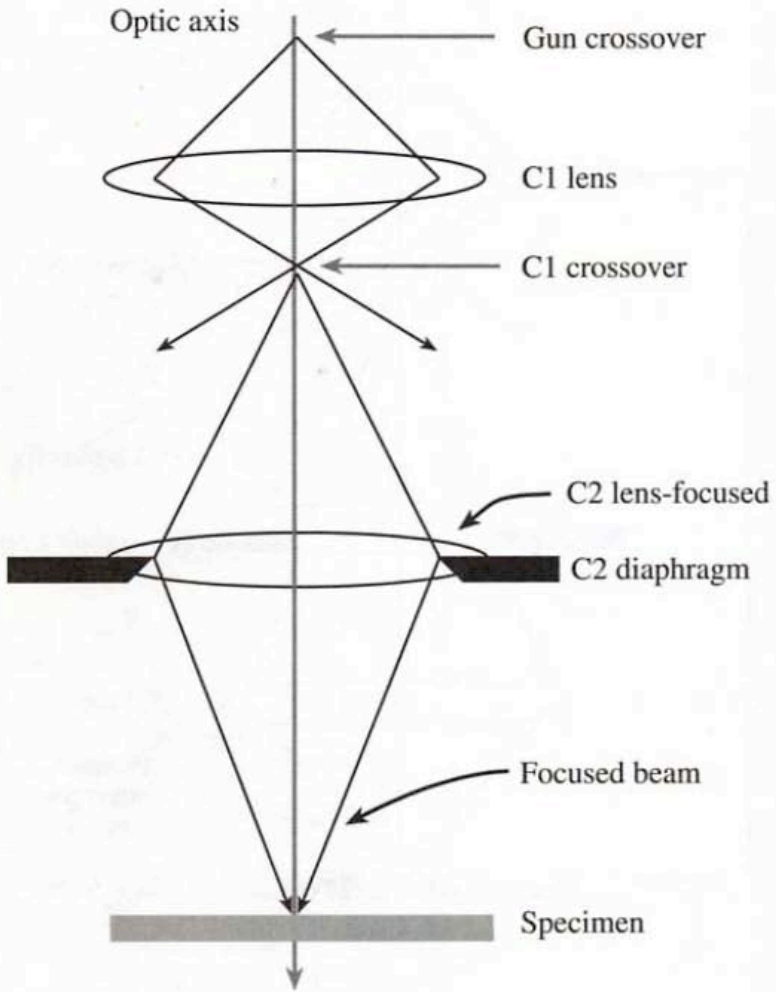

Figure 9.3. A focused C2 lens illuminates a small area of the specimen with a nonparallel beam.

Electron Diffraction

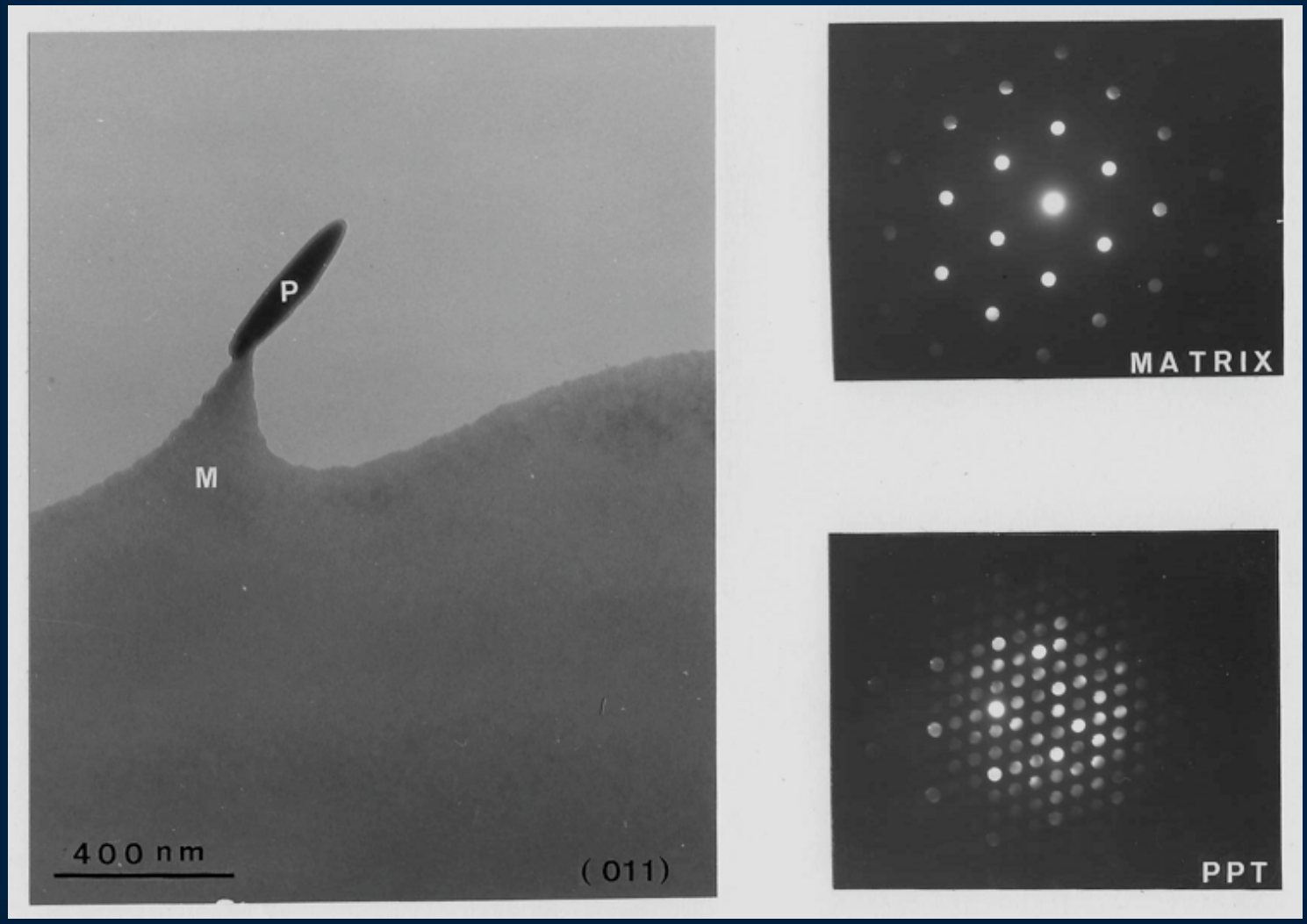

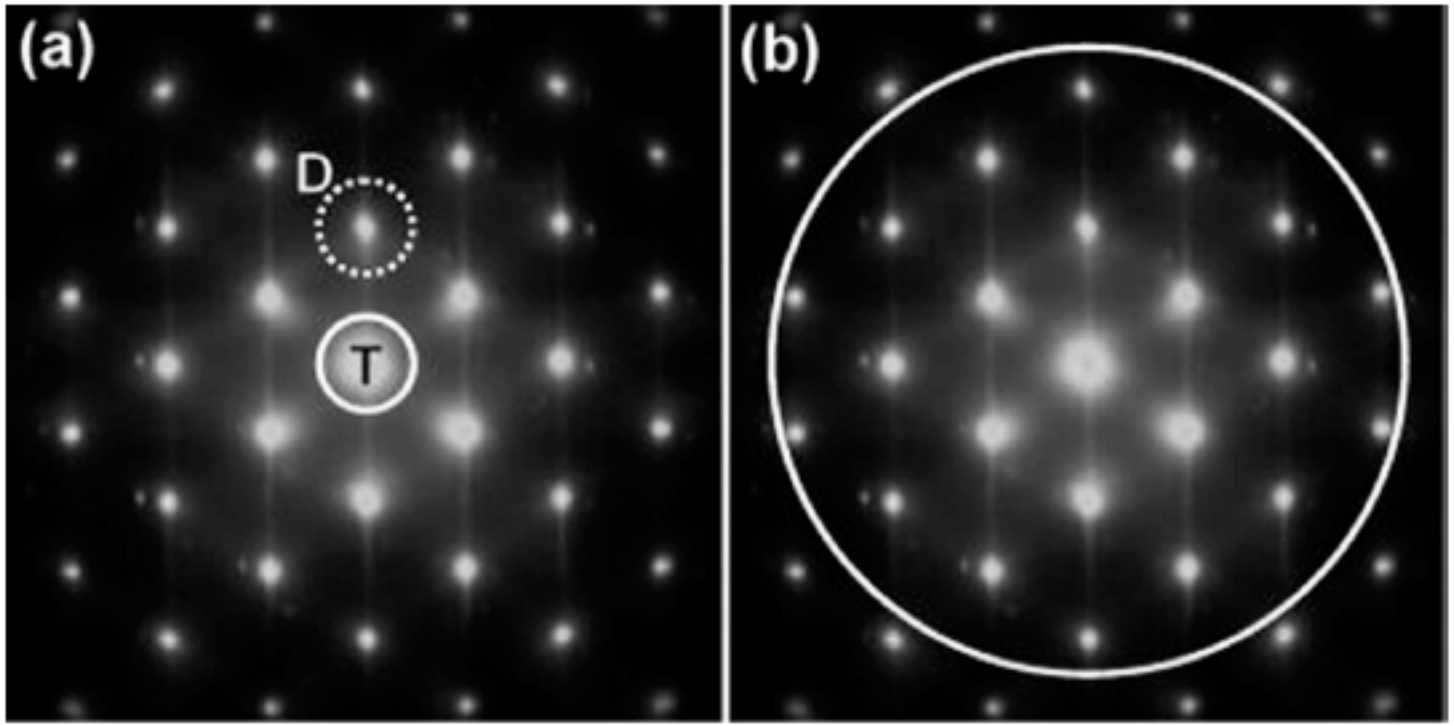
(a)
D
T
(b)

Obtaining ~ Parallel Illumination

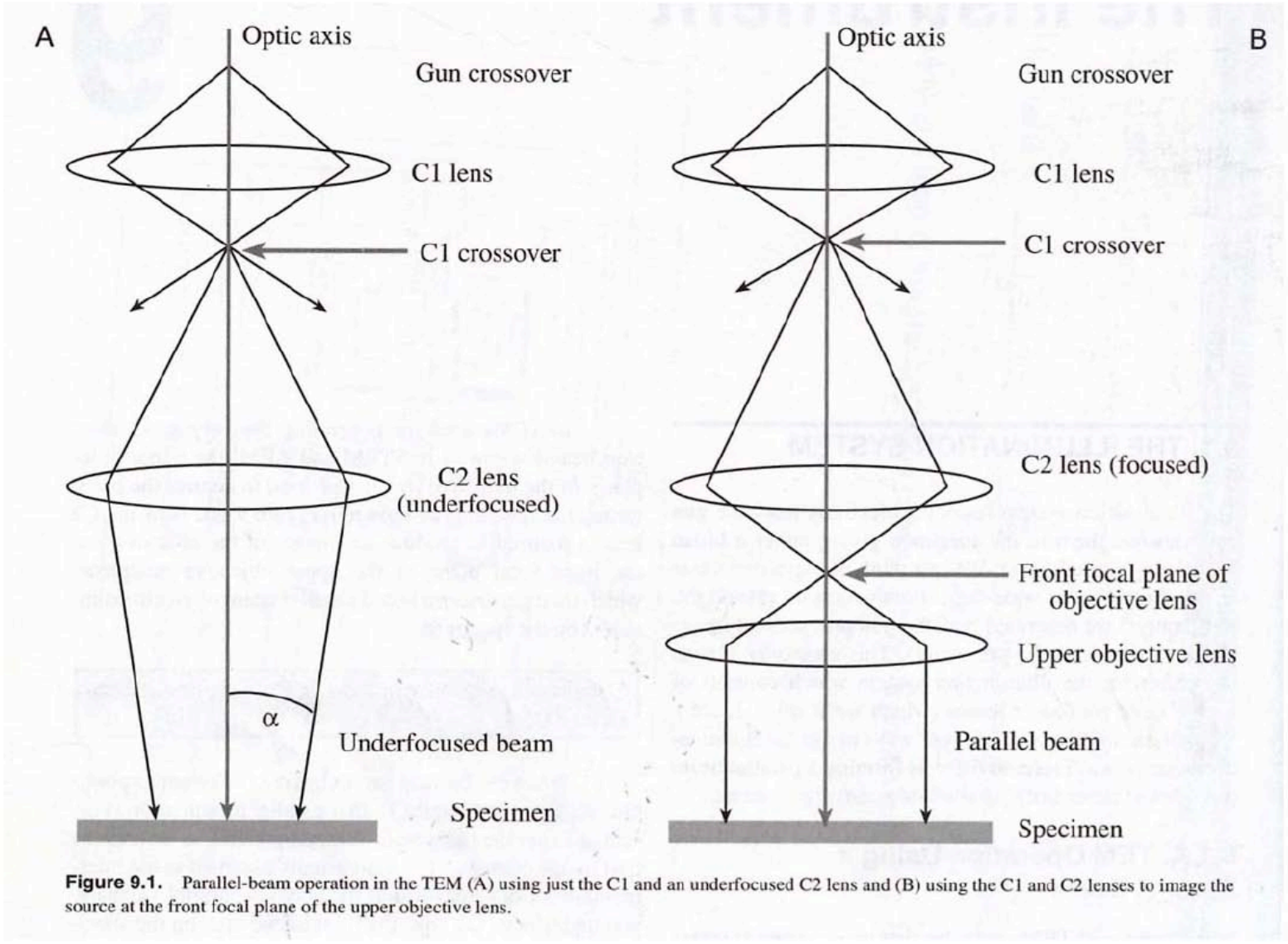

Figure 9.1. Parallel-beam operation in the TEM (A) using just the C1 and an underfocused C2 lens and (B) using the C1 and C2 lenses to image the source at the front focal plane of the upper objective lens.

Place an aperture in the Image Plane this defines an area back projected onto the specimen

Selected-Area Diffraction

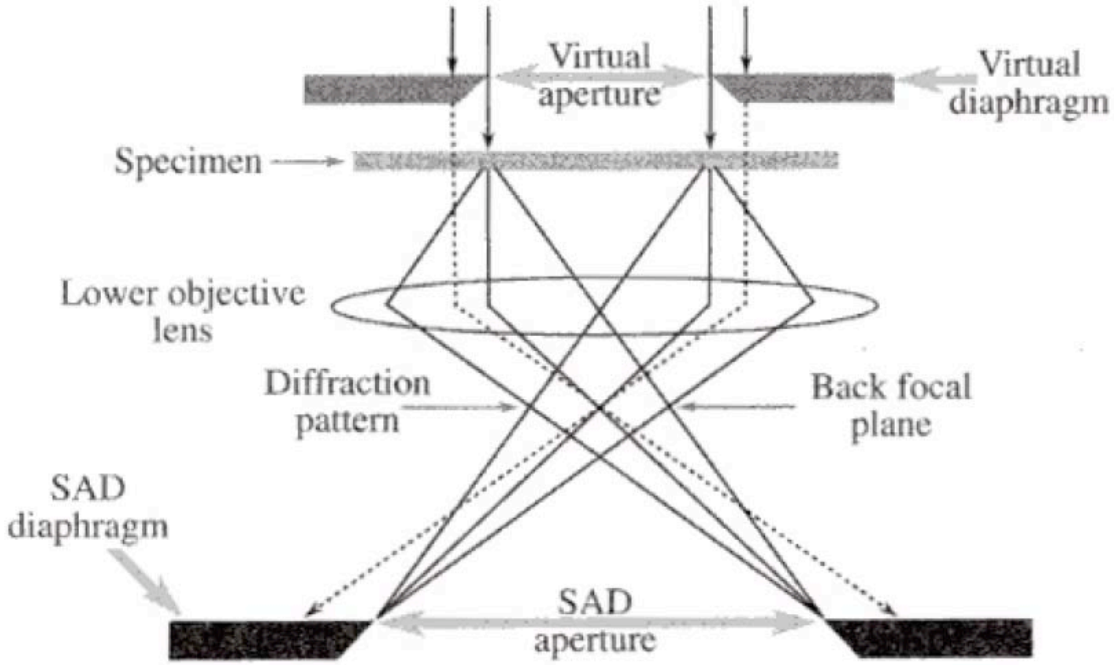

Figure 9.13. Ray diagram showing SAD pattern formation: the insertion of an aperture in the image plane results in the creation of a virtual aperture in the plane of the specimen. Only electrons falling inside the dimensions of the virtual aperture at the specimen will be allowed through into the imaging system. All other electrons will hit the SAD diaphragm.

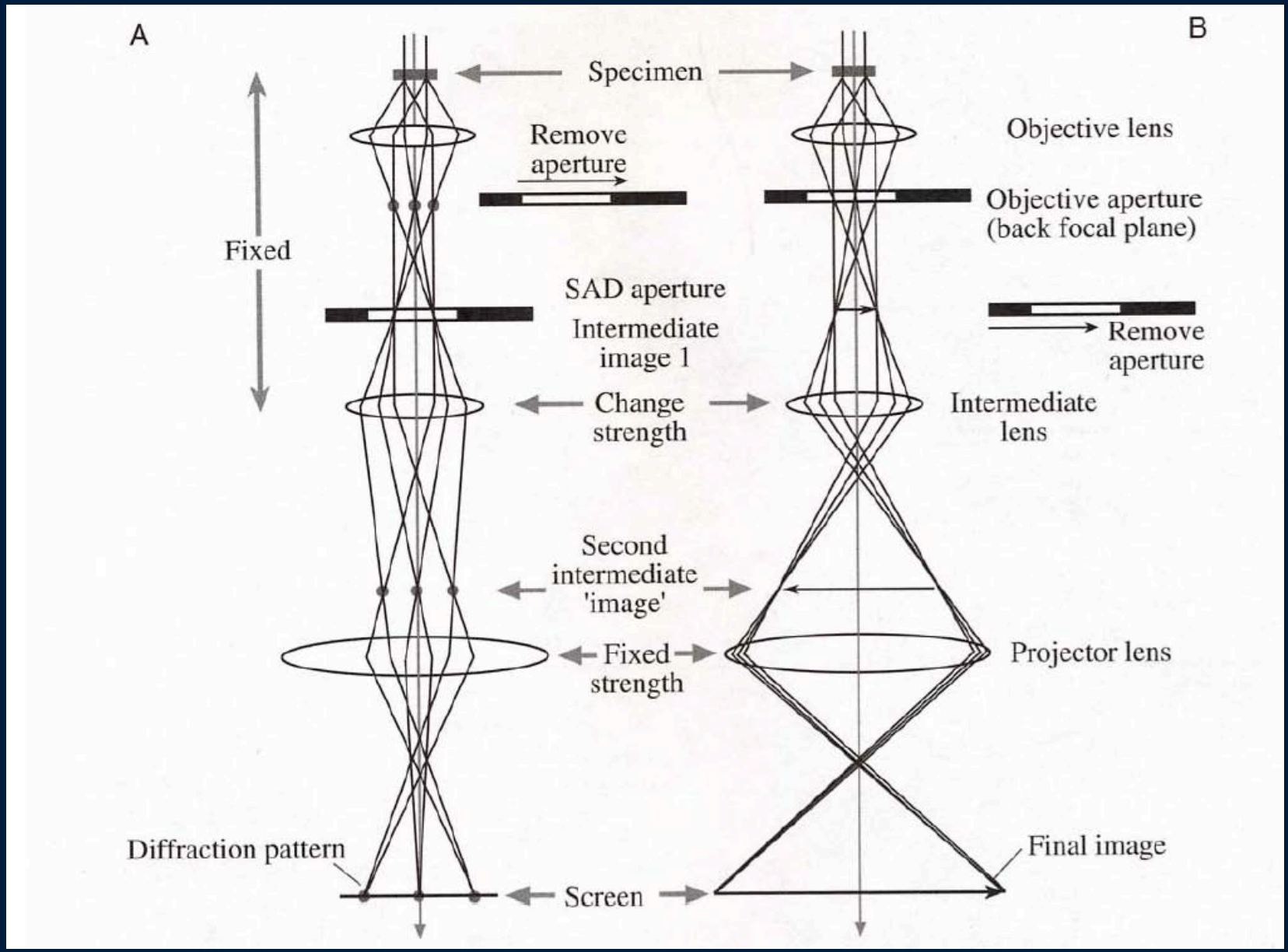
A
B
Specimen
Remove aperture
Objective lens
Objective aperture (back focal plane)
Fixed
SAD aperture
Intermediate image 1
Remove aperture
Change strength
Intermediate lens
Second intermediate 'image'
Fixed strength
Projector lens
Diffraction pattern
Screen
Final image

Why CBED? Why not SAD?

Limits of Conventional SAD

Conventional SAD uses an aperture to define the area from which the pattern is to be recorded. The aperture is placed in the image plane of the objective lens to create a virtual aperture in the specimen plane (Le Poole 1947). The spatial resolution in SAD is limited by both spherical aberration and the ability of the operator to focus the aperture of the and the image in the same plane. The error in area selection U is given by:

$$U = C_s(2\theta_B)^3 + D2\theta_B$$

where: C_s ***= spherical aberration coefficient***

θ_B ***= Bragg angle***

D= minimum focus step.

The result is that the theoretical lower limit of area selection is ~0.5μm (in practice governed by aperture size).

J.B. Le Poole, Philips Tech. Rundsch 9 (1947) 33.

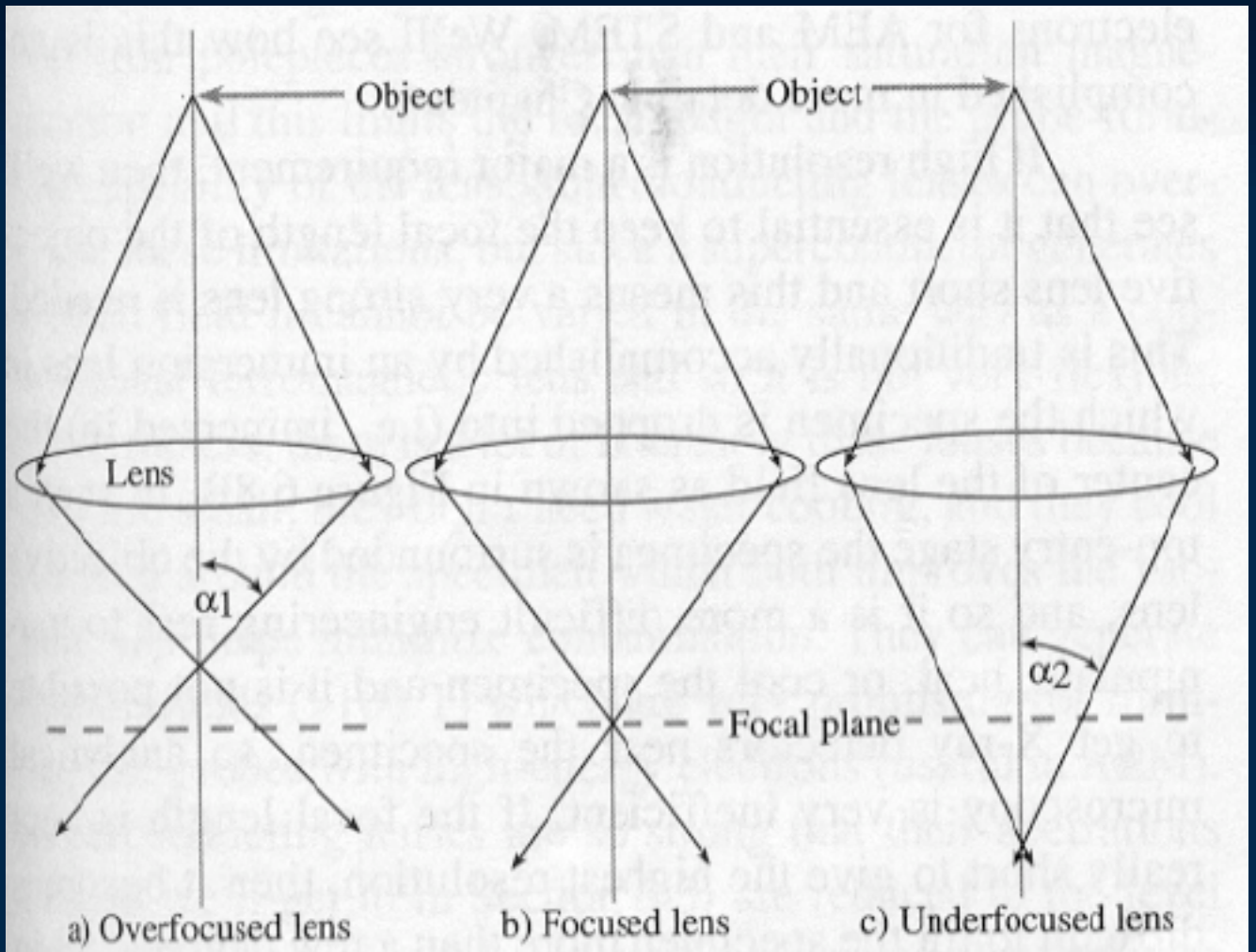

Figure 6.5. (a) Ray diagram illustrating the concepts of overfocus, in which a strong lens focuses the rays before the image plane, and (c) underfocus, where a weaker lens focuses after the image plane. It is clear from (c) that at a given underfocus the convergent rays are more parallel than the equivalent divergent rays at overfocus ($\alpha_2 < \alpha_1$).

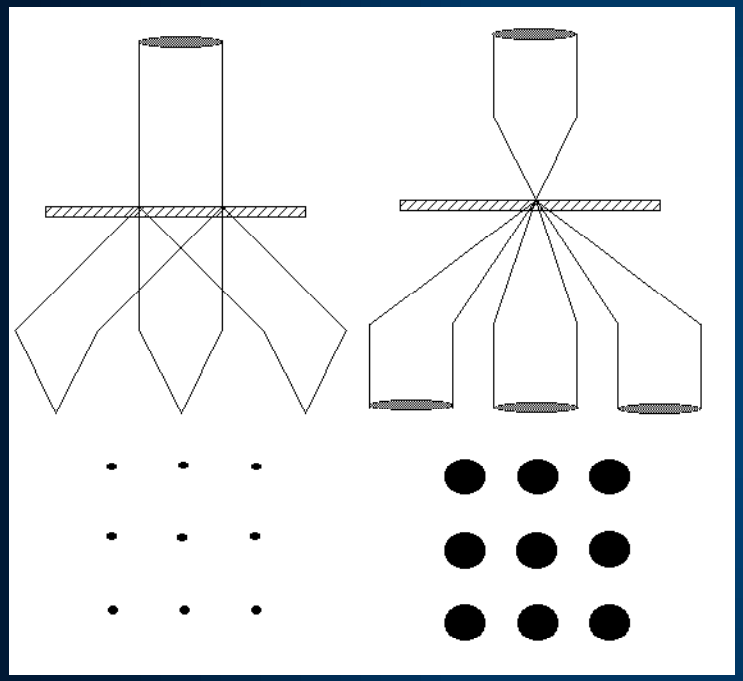

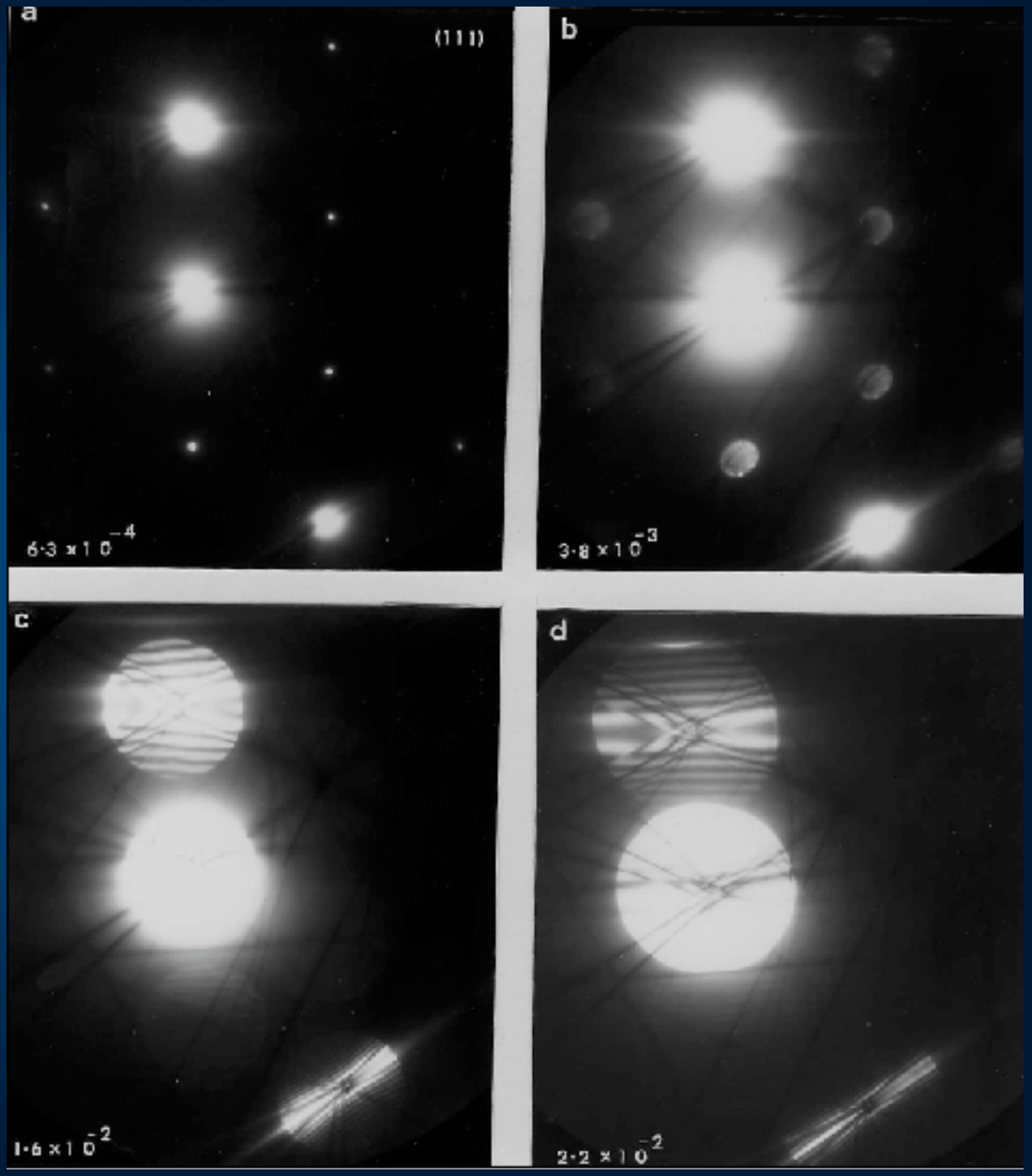

Notice, loss of definition of weak reflections !

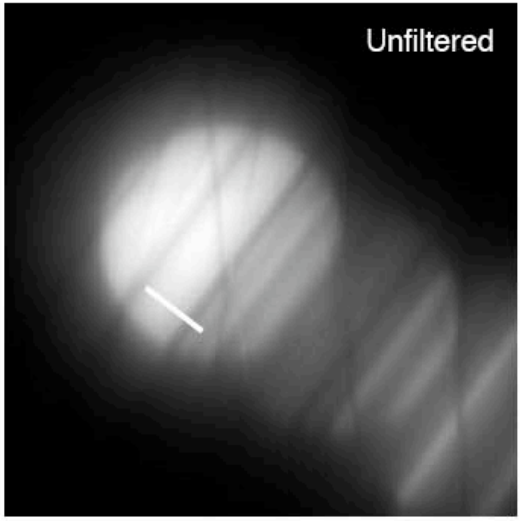

Silicon [110]

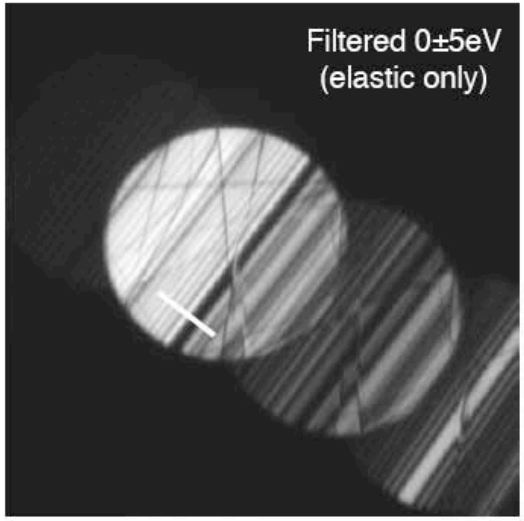

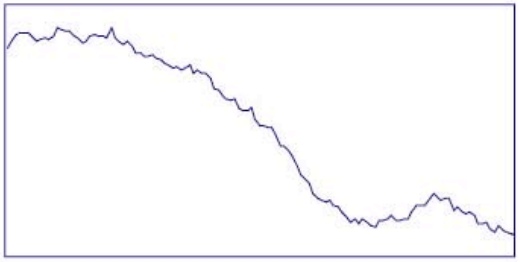

essential for
quantitative CBED

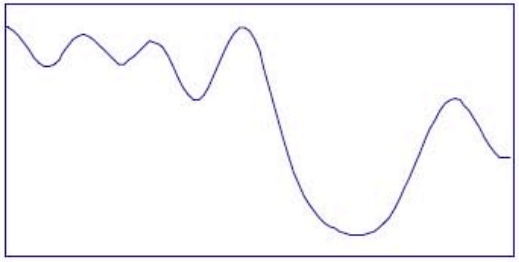

Silicon 111 ZAP- Energy Filtered

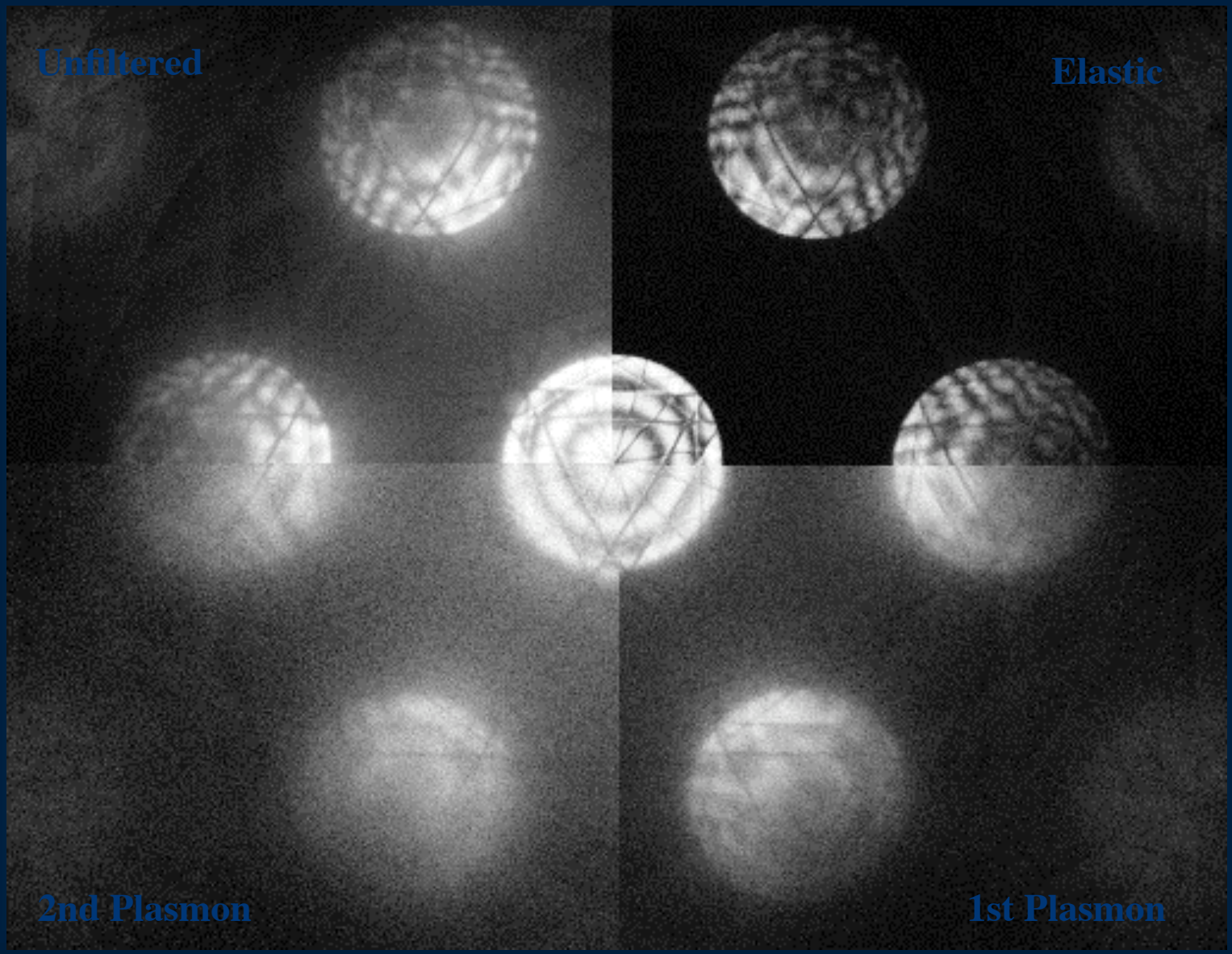

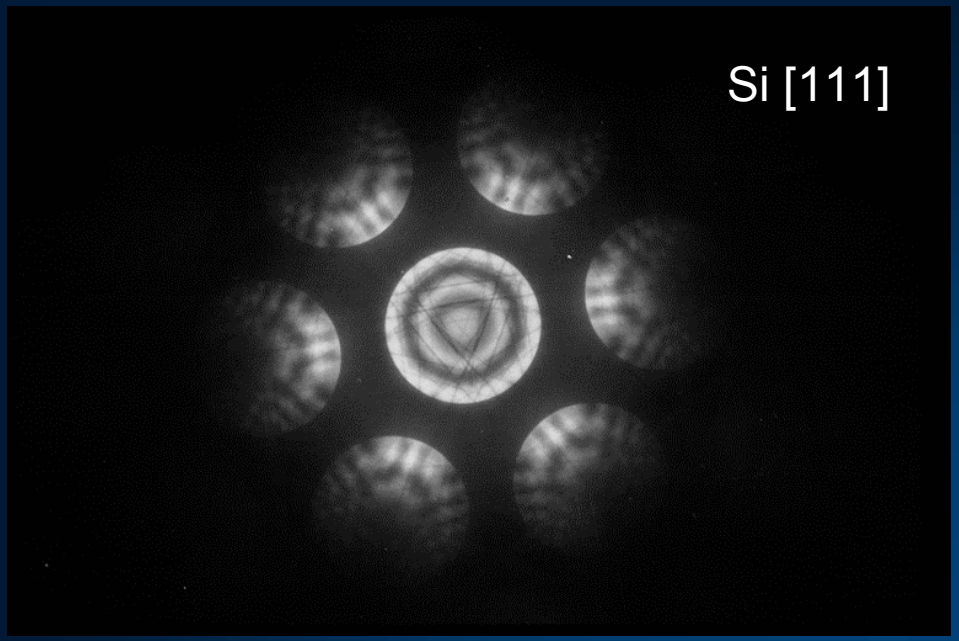

CBED is extremely sensitive to orientation and is the best way to set the exact orientation

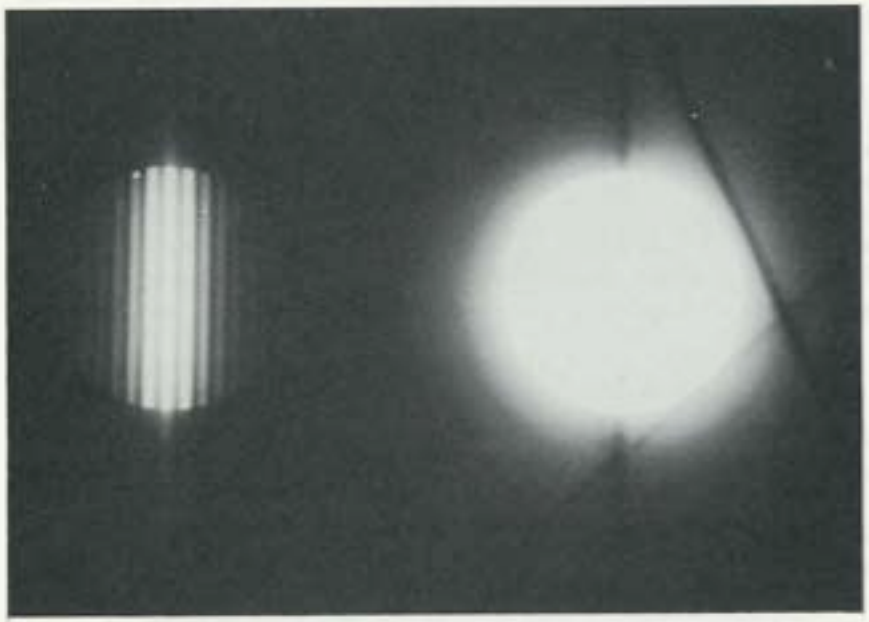

(a)

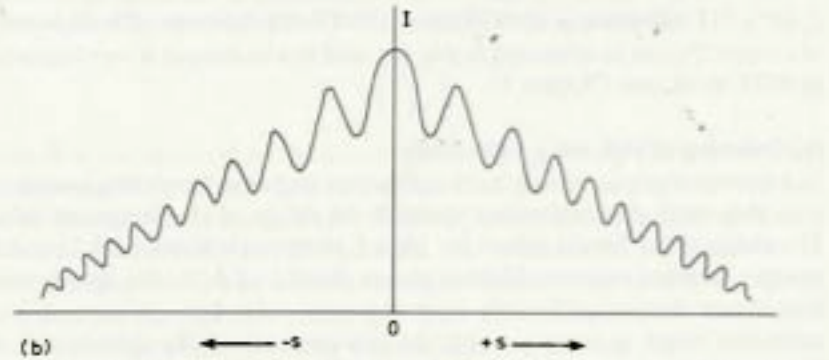

Fig. 4.9 (a) Magnified image of a convergent beam diffraction pattern taken from aluminium at 120 kV. The diffracted beam shows minima corresponding to those in (b). The precise positions of the minima depend on the foil thickness (cf. equation (4.5)).

Theoretical Considerations for Thickness Measurement

Convergent beam diffraction discs are maps of diffracted intensity as a function of incident wave angle and therefore have a direct correspondence to a rocking curve. In the two-beam approximation the rocking curve for the diffracted intensity $|\phi|^2$ is given by (Hirsch et al. 1965):

$$|\phi|^2 = \sin^2 \beta\pi\Delta k z \qquad (1)$$

Where:

$$\beta = \tan^{-1}\left(\frac{1}{s\xi_g}\right) \quad \Delta k = \frac{\sqrt{1+(s\xi_g)^2}}{\xi_g}$$

s is the deviation parameter, ξ_g is the extinction distance and z the foil thickness.

"Electron Microscopy of Thin Crystals", Hirsch et al (1965).

Differentiation with respect to s reveals that the minima of $|\phi|^2$ in equation (1) obey the relationship:

$$\Delta kz = \text{integer} \quad (2a)$$

and the maxima obey the relationship:

$$\tan \pi \Delta kz = \pi \Delta kz \quad (2b)$$

Also, s=0 is always either a maximum or minimum. Kelly et al. (1975) expressed equation (2a) as:

$$(\frac{s_i}{n_k})^2 = -(\frac{1}{\xi})^2(\frac{1}{n_k})^2 + (\frac{1}{z})^2 \quad (3a)$$

It is evident that a plot of $(\frac{s_i}{n_k})^2$ against $(\frac{1}{n_k})^2$ in a two-beam condition yields a straight line with intercept $(\frac{1}{z})^2$ and slope of $(\frac{1}{\xi})^2$. This is the basis of the CBED thickness measurement technique that is now well known.

P.M. Kelly et al., Phys. Stat. Sol. (1975)A31, 771.

Si <220> @ 200 kV
a=0.543 nm
t~ 280 nm ξ ~ 125 nm

$$\left(\frac{s_i}{x_{k'}}\right)^2=-\left(\frac{1}{\xi}\right)^2\left(\frac{1}{x_{k'}}\right)^2+\left(\frac{1}{z}\right)^2$$

Equation for sequence of maxima where:

$$s_i=\frac{\lambda}{d^2}\frac{\Delta\theta}{2\theta_d}$$

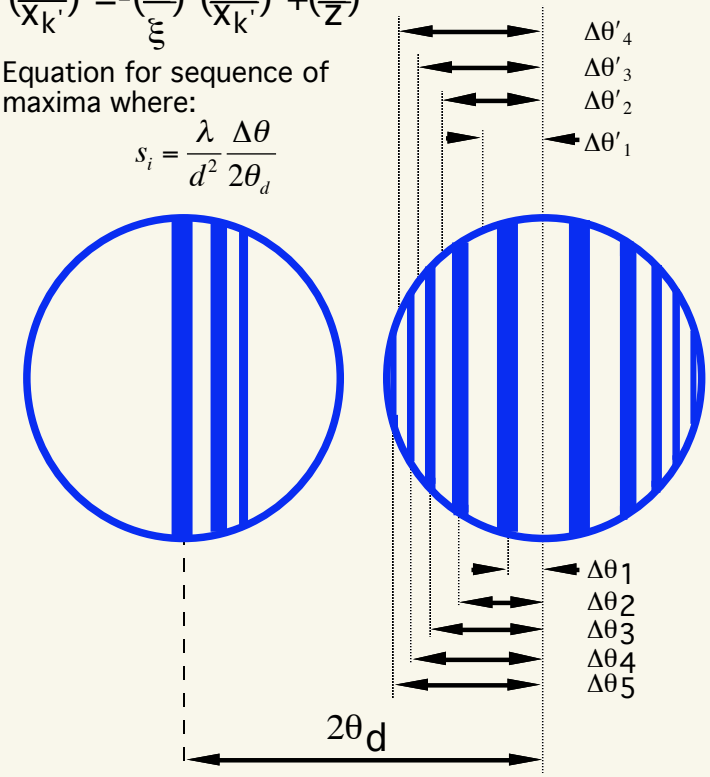

$$\left(\frac{s_i}{n_k}\right)^2=-\left(\frac{1}{\xi}\right)^2\left(\frac{1}{n_k}\right)^2+\left(\frac{1}{z}\right)^2$$

Equation for sequence of minima where:

$$s_i=\frac{\lambda}{d^2}\frac{\Delta\theta}{2\theta_d}$$

$$\left(\frac{s_i}{n_k}\right)^2=-\left(\frac{1}{\xi}\right)^2\left(\frac{1}{n_k}\right)^2+\left(\frac{1}{z}\right)^2$$

Points for minima open squares

Intercept $\frac{1}{z^2}$

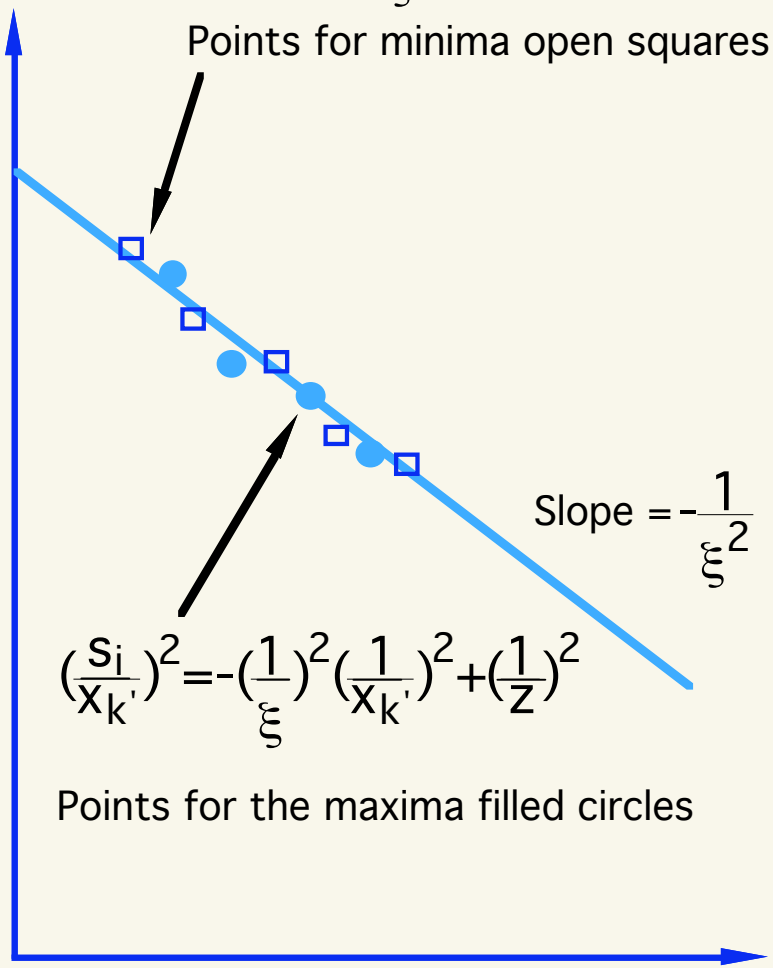

Slope $=-\frac{1}{\xi^2}$

$$\left(\frac{s_i}{x_{k'}}\right)^2=-\left(\frac{1}{\xi}\right)^2\left(\frac{1}{x_{k'}}\right)^2+\left(\frac{1}{z}\right)^2$$

Points for the maxima filled circles

Diffracted Intensity Falls off with angle because of Ewald Sphere

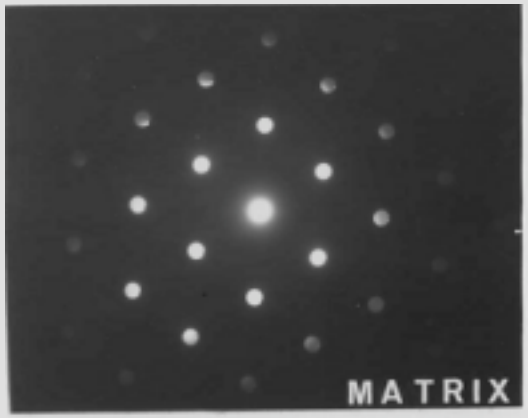

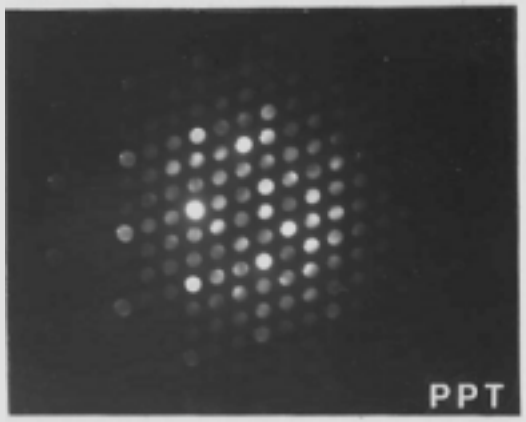

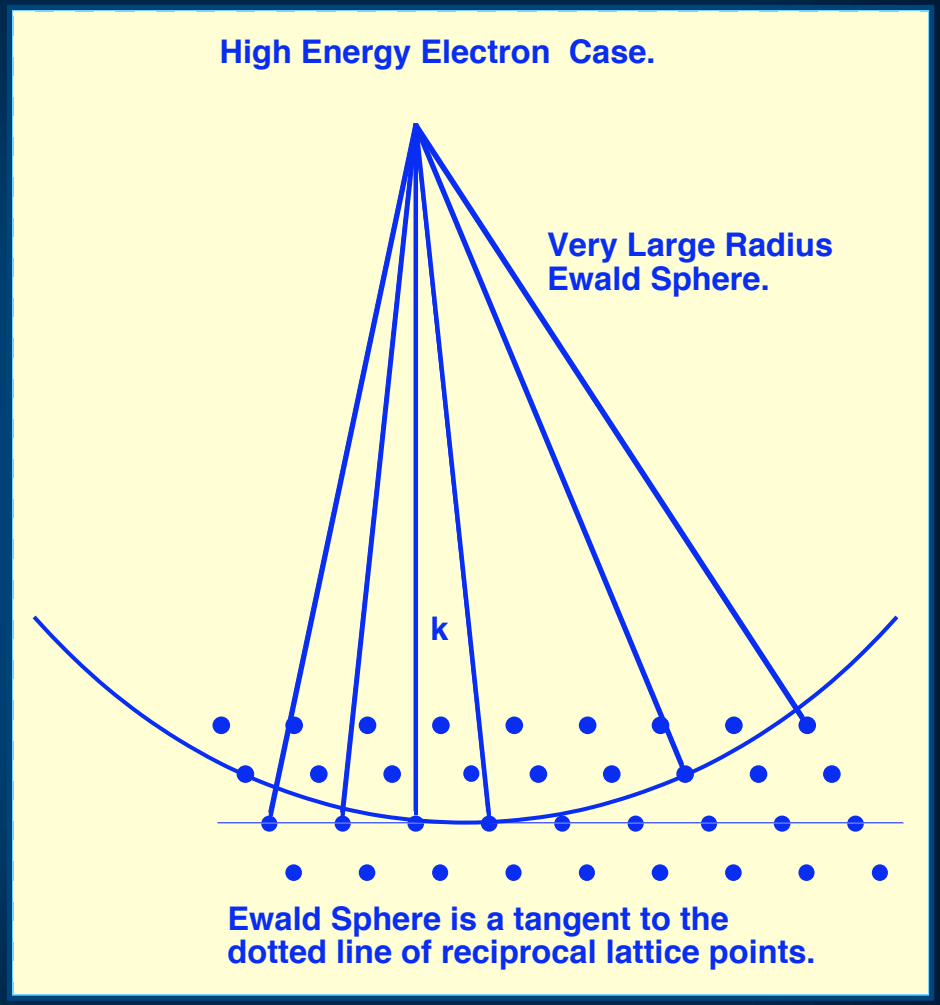

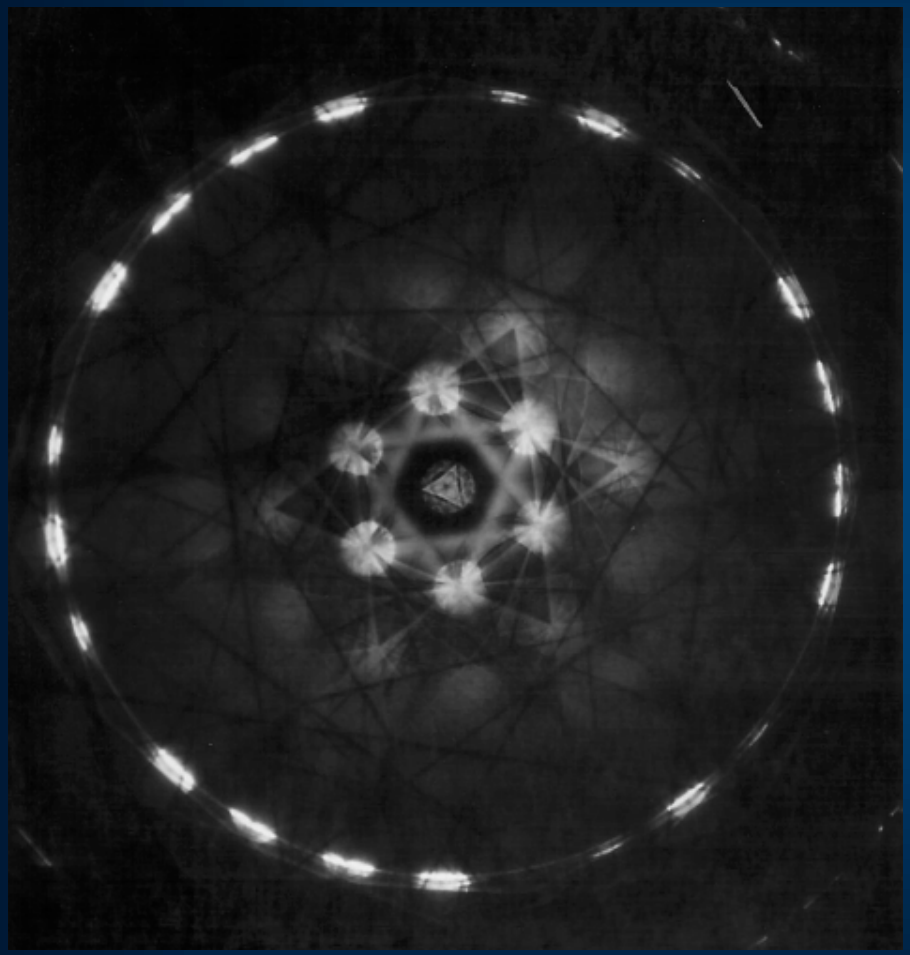

Laue Zones

- At a zone-axis orientation, the reflections in the diffraction pattern break up into zones called Laue zones
- The central zone is called the zero-order Laue zone
- The first ring is called the first-order Laue zone - and so on
- The first-order, second-order, third order (and so on) are known collectively as the higher-order Laue zones

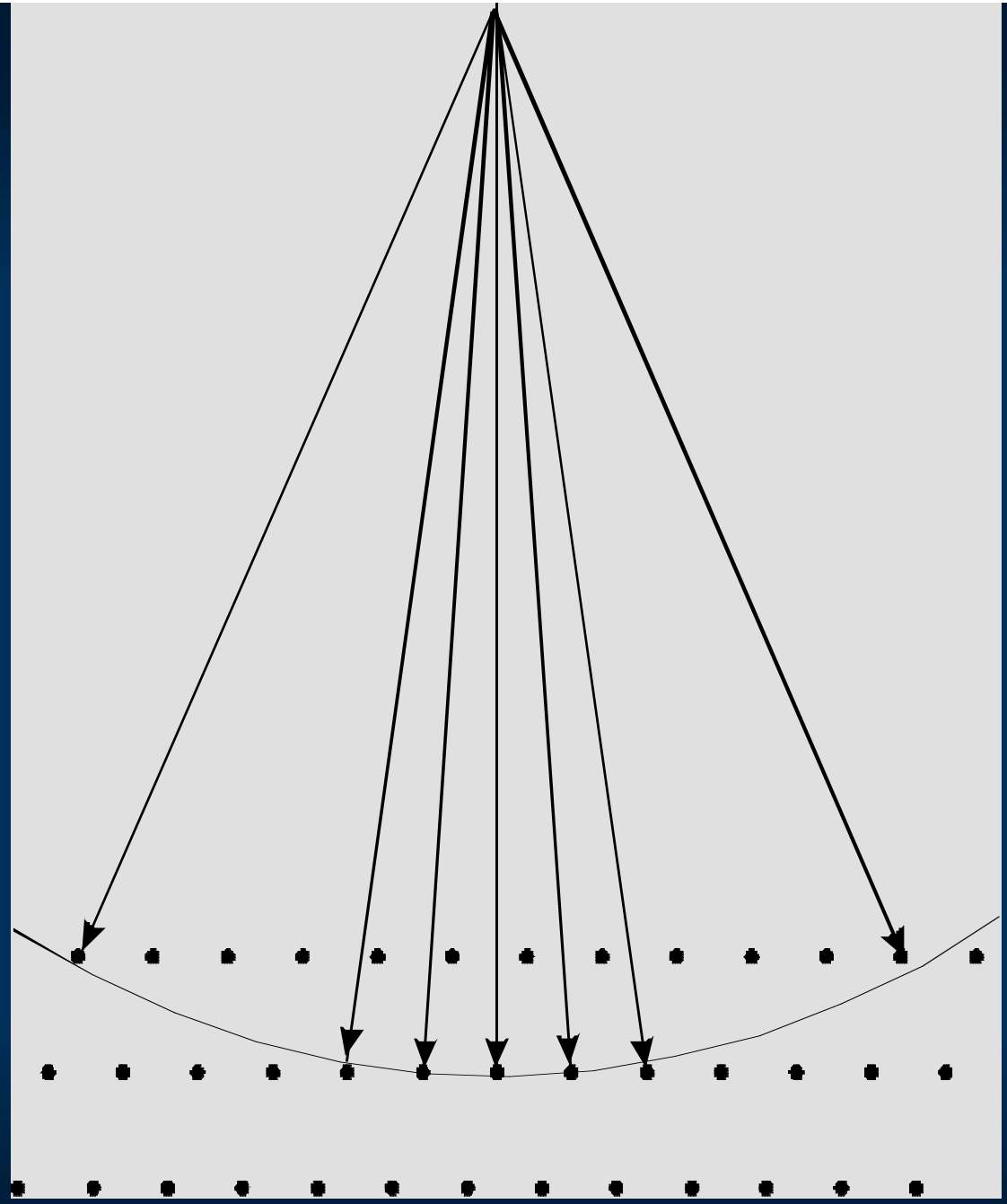

HOLZ

- HOLZ is the acronym for higher-order Laue zone
- The rings of reflections outside the central, zero-order Laue zone are the HOLZ
- Because the narrow, dark, straight lines in the bright field disc are associated with diffraction into a HOLZ reflection, they are known as HOLZ lines
- Do not confuse HOLZ with HOLZ lines

Formation of HOLZ rings.

If $H^2 \rightarrow 0$

$G_1 = \sqrt{2kH}$

$G_2 = 2\sqrt{kH}$

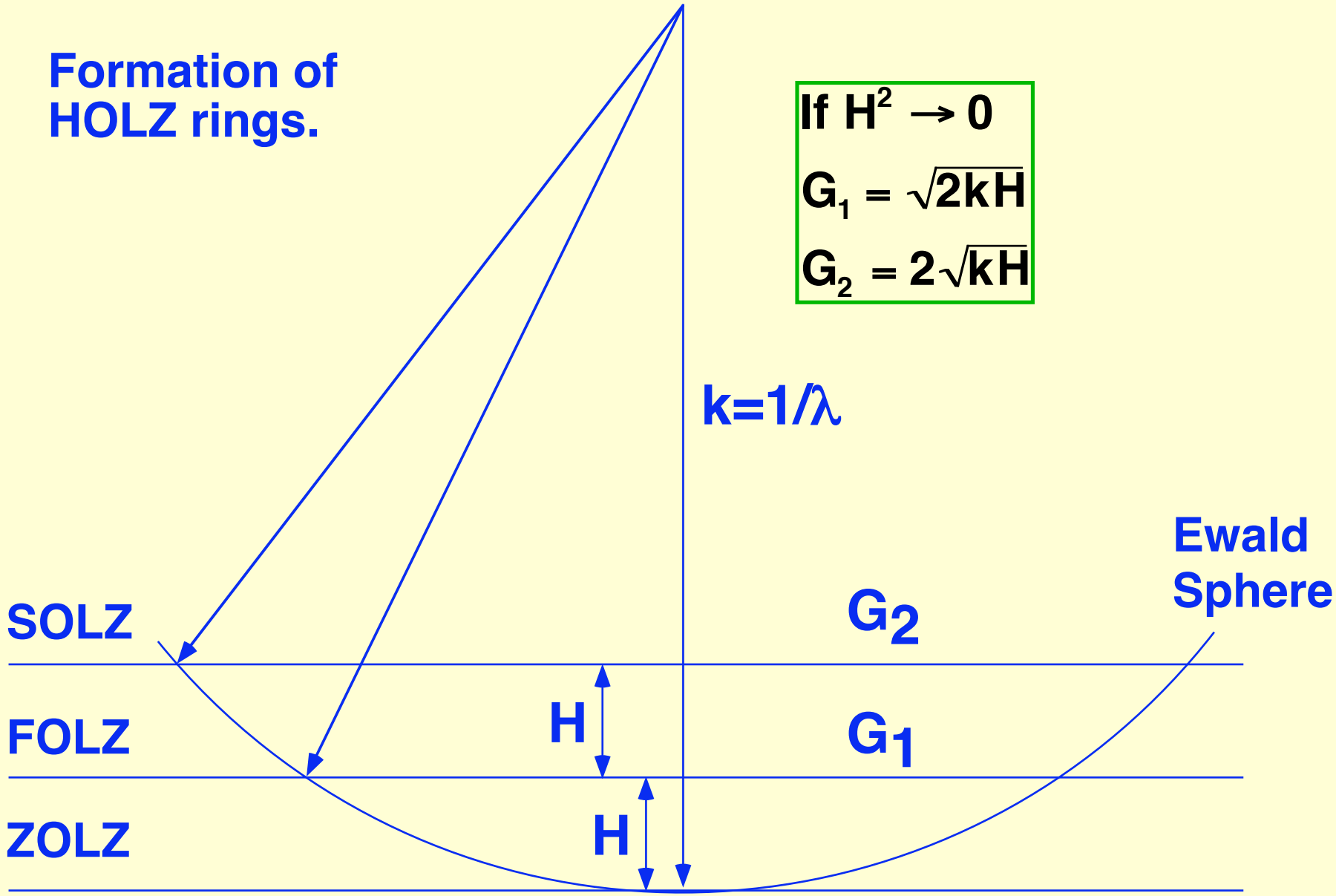

ZOLZ or Zero Layer.

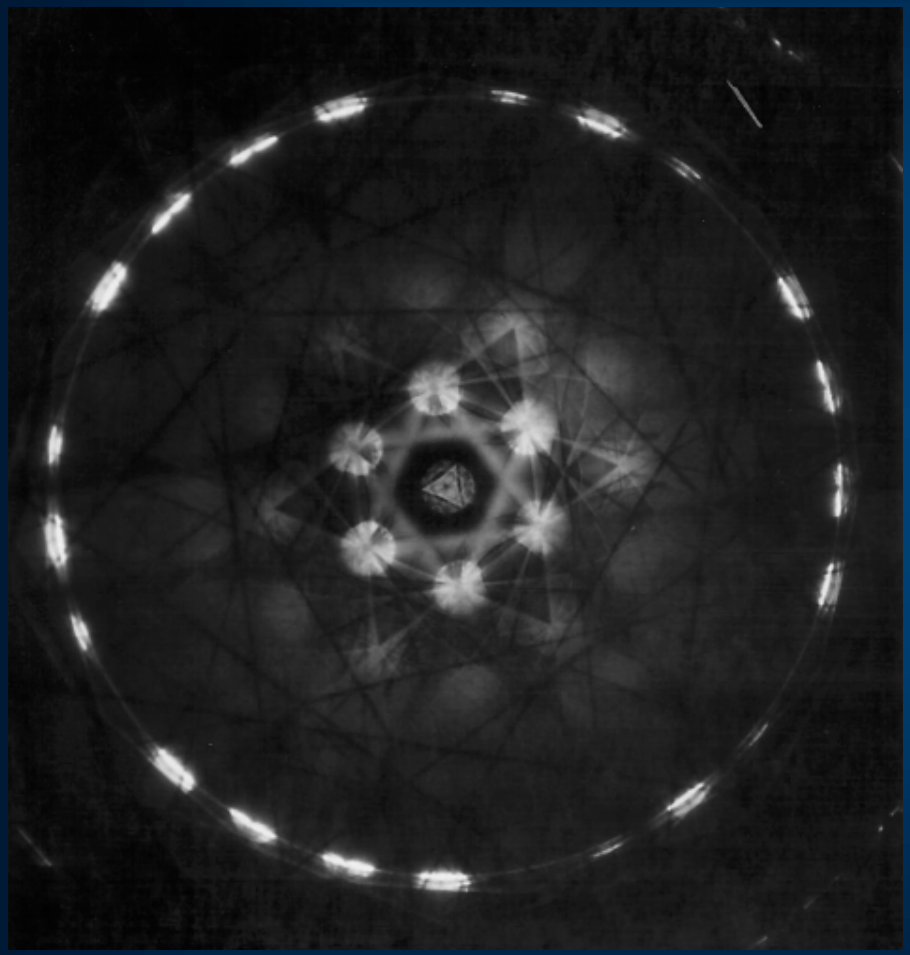

Relation between the diffraction groups and the crystal point groups

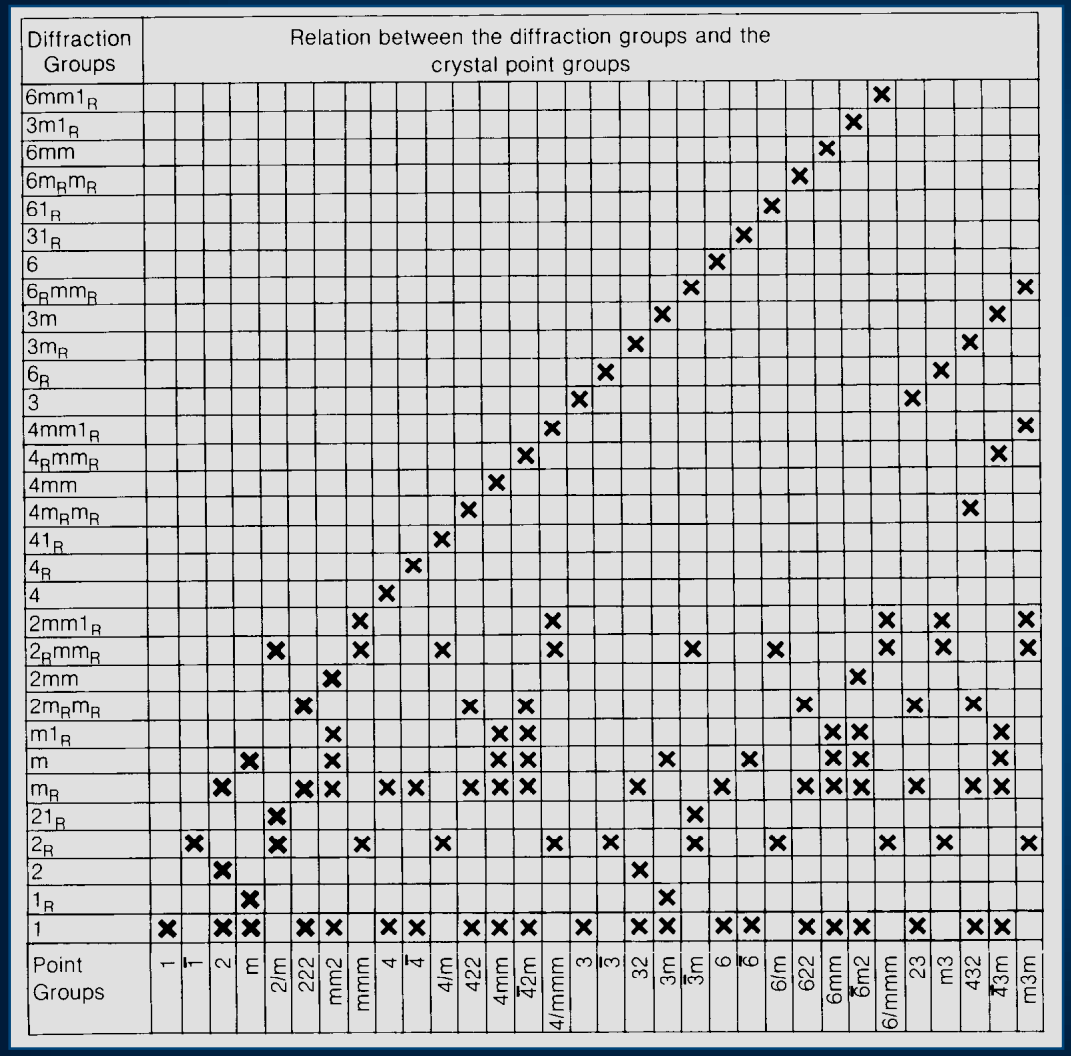

Originally from Buxton et al (1976) Phil. Trans. Roy. Soc. 281, 181.

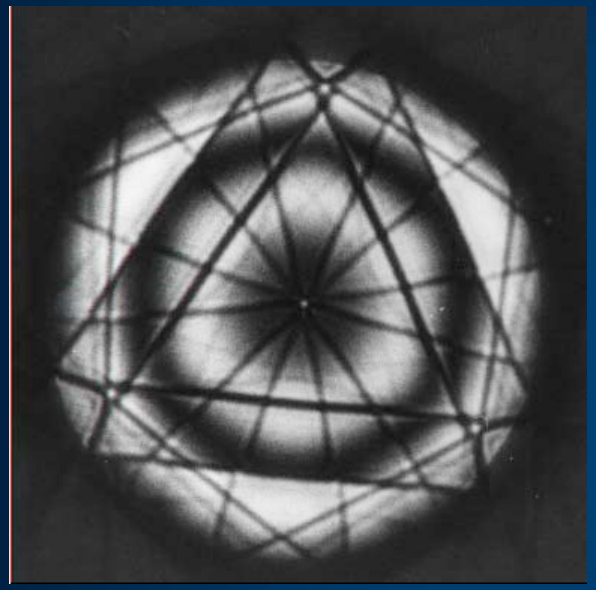

113 kV

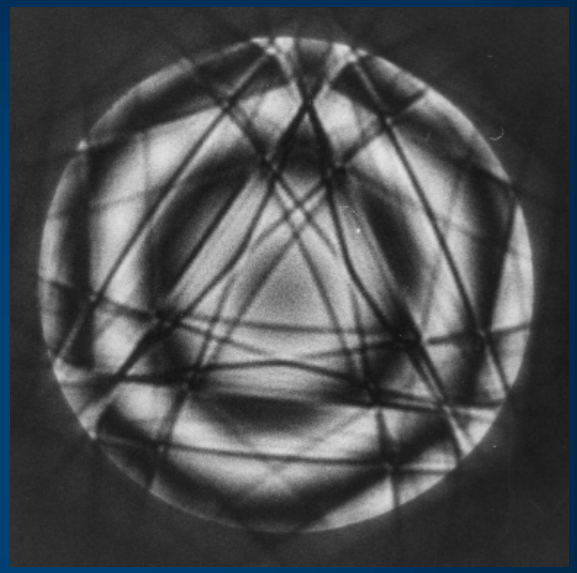

100 kV

<001> CBED ZAPs from Si & SiGe Alloys

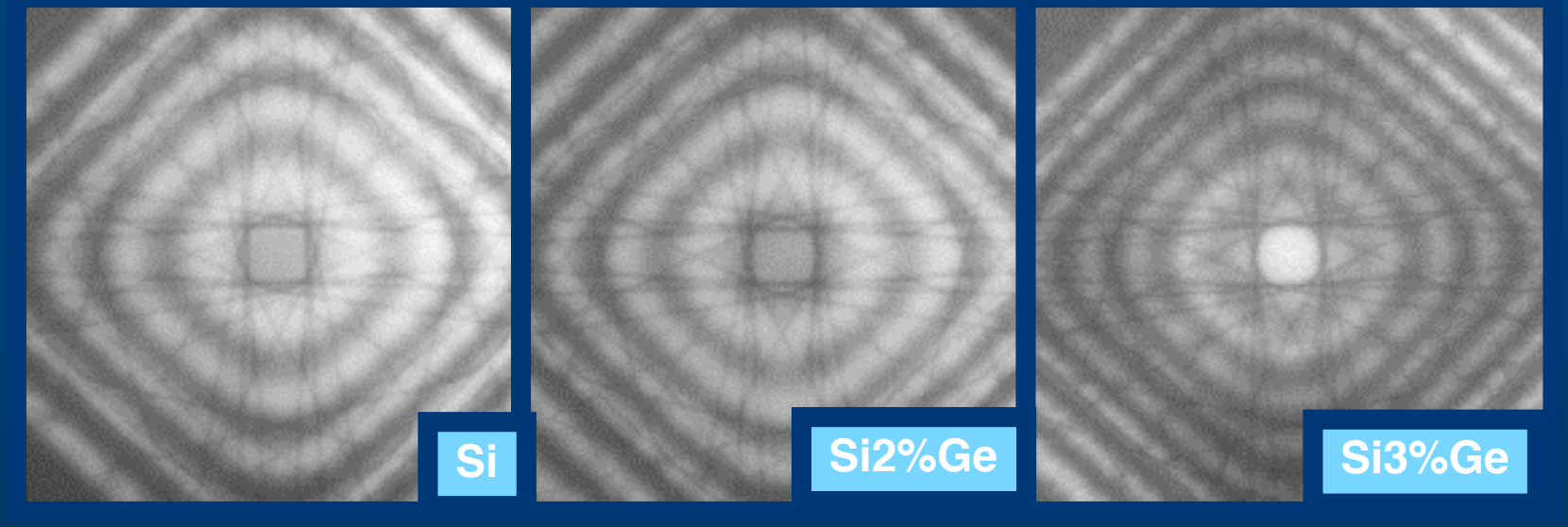

CBED ZAPs from Si, Si2%Ge & Si3%Ge cross section samples. Center of direct disc. Patterns recorded at 150kV, with a beam convergence of ~8mrad. Probe diameter ~30nm. Samples were held at liquid nitrogen temperature to reduce the thermal diffuse scattering. The orthorhombic distortion of the lattice is most obvious in the Si2%Ge sample.

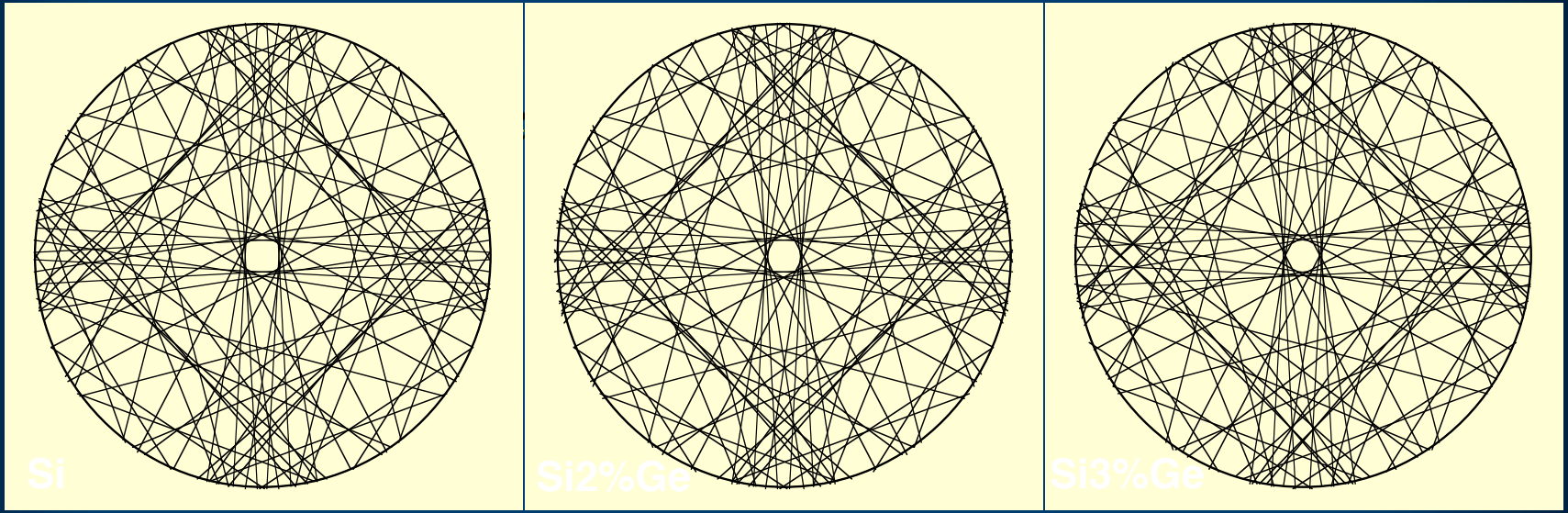

CBED Simulations based on the kinematical approximation for Si, Si2%Ge and Si3%Ge. <001> zone axis pattern, convergence angle approximately 10mrad. Voltage set to 149.5kV by comparison with the Si pattern.
Lattice parameters:
Silicon a=0.5429nm, Si2%Ge a=0.5434nm b= 0.5429nm c= 0.5430nm
Si3%Ge a= 0.5445nm b= 0.5440nm c= 0.5440nm

HOLZ Plots
generated by Diffract™